

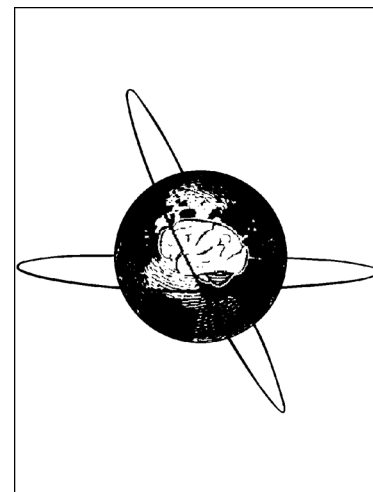
Standardized hierarchical adaptive L_p regression for noise robust focal epilepsy source reconstructions

Joonas Lahtinen, Alexandra Koulouri, Stefan Rampp, Jörg Wellmer, Carsten Wolters, Sampsa Pursiainen

PII: S1388-2457(23)00797-6
DOI: <https://doi.org/10.1016/j.clinph.2023.12.001>
Reference: CLINPH 2010333

To appear in: *Clinical Neurophysiology*

Accepted Date: 2 December 2023




Please cite this article as: Lahtinen, J., Koulouri, A., Rampp, S., Wellmer, J., Wolters, C., Pursiainen, S., Standardized hierarchical adaptive L_p regression for noise robust focal epilepsy source reconstructions, *Clinical Neurophysiology* (2023), doi: <https://doi.org/10.1016/j.clinph.2023.12.001>

This is a PDF file of an article that has undergone enhancements after acceptance, such as the addition of a cover page and metadata, and formatting for readability, but it is not yet the definitive version of record. This version will undergo additional copyediting, typesetting and review before it is published in its final form, but we are providing this version to give early visibility of the article. Please note that, during the production process, errors may be discovered which could affect the content, and all legal disclaimers that apply to the journal pertain.

Highlights

1. We extended the theory of the sLORETA standardization to make it applicable to a class of hierarchical Bayesian methods.
2. Applying standardization to hierarchical adaptive L1 regression, we obtain increased localization accuracy and noise robustness.
3. With the new L1 regularized method, we found the epileptic sources within 1 cm accuracy in epilepsy patients.

Standardized hierarchical adaptive L_p regression for noise robust focal epilepsy source reconstructions

Joonas Lahtinen ^{a,*}, Alexandra Koulouri^a, Stefan Ramm^{b,c,d}, Jörg Wellmer^e, Carsten Wolters^{f,g}, Sampsa Porsiaainen^a

^aFaculty of Information Technology and Communication Sciences, Tampere University, Tampere, 33720, Finland

^bDepartment of Neurosurgery, University Hospital Halle (Saale), Halle, 06097, Germany

^cDepartment of Neurosurgery, University Hospital Erlangen, Erlangen, 91054, Germany

^dDepartment of Neuroradiology, University Hospital Erlangen, Erlangen, 91054, Germany

^eRuhr-Epileptology, Department of Neurology, University Hospital Knappschaftskrankenhaus, Ruhr-University, Bochum, 44892, Germany

^fInstitute for Biomagnetism and Biosignalanalysis, University of Münster, Münster, 48149, Germany

^gOtto Creutzfeldt Center for Cognitive and Behavioral Neuroscience, University of Münster, Münster, 48149, Germany

Abstract

Objective: To investigate the ability of standardization to reduce source localization errors and measurement noise uncertainties for hierarchical Bayesian algorithms with L_1 - and L_2 -norms as priors in electroencephalography and magnetoencephalography of focal epilepsy.

Methods: Description of the standardization methodology relying on the Hierarchical Bayesian framework, referred to as the Standardized Hierarchical Adaptive L_p -norm Regularization (SHALpR).

The performance was tested using real data from two focal epilepsy patients. Simulated data that resembled the available real data was constructed for further localization and noise robustness investigation.

Results: The proposed algorithms were compared to their non-standardized counterparts, Standardized low-resolution brain electromagnetic tomography, Standardized Shrinking LORETA-FOCUSS, and Dynamic statistical parametric maps. Based on the simulations, the standardized Hierarchical adaptive algorithm using L_2 -norm was noise robust for 10 dB signal-to-noise ratio (SNR), whereas the L_1 -norm prior worked robustly also with 5 dB SNR. The accuracy of the standardized L_1 -normed methodology to localize focal activity was under 1 cm for both patients.

Conclusions: Numerical results of the proposed methodology display improved localization and noise robustness. The proposed methodology also outperformed the compared methods when dealing with real data.

Significance: The proposed standardized methodology, especially when employing the L_1 -norm, could serve as a valuable assessment tool in surgical decision-making.

Keywords: Hierarchical Bayesian model, EEG/MEG, Focal epilepsy, Standardization, Source localization


1. Introduction

In drug-resistant (refractory) epilepsy, resective surgery is seen as a viable treatment option that can achieve seizure-freedom as the best outcome (Engel, 1996; Lüders et al., 2006; Conte et al., 2018). A successful surgery outcome proceeds from a successful localization of epilepsy source (ES) as a part of presurgical evaluation (Rosenow and Lüders, 2001; Zijlmans et al., 2019; Murakami et al., 2016). While invasive electroencephalography (iEEG) recordings are preferred from the standpoint of spatial precision (Engel Jr et al., 1981), those are limited to small brain volumes, and therefore, are only able to define the seizure onset zone when

covering it (Coito et al., 2019). The location of ES can be estimated non-invasively using electroencephalography (EEG) and magnetoencephalography (MEG) recordings of interictal or ictal activity on the scalp (Diamond et al., 2023; Mouthaan et al., 2019; Plummer et al., 2008). Epileptic activity is often estimated from averaged spikes (Leal et al., 2008; Lie et al., 2015; Eom et al., 2016; Mouthaan et al., 2019). Either a realistic head model (Feng et al., 2016; Aydin et al., 2017; Neugebauer et al., 2022) or simplistic spherical model (Bast et al., 2006; Brodbeck et al., 2011; de Gooijer-van de Groep et al., 2013; Mégevand et al., 2014; Hall et al., 2018; Cai et al., 2021) can be used in source estimation. Naturally, the better the model of the patient's head, the greater the accuracy of the source localization can be (Roth et al., 1993; Vanrumste et al., 2002; Vatta et al., 2010). For that reason, we use realistic head models constructed using magnetic resonance imaging (MRI) data gathered from the patients.

Estimation of ES is often a difficult task which is highlighted by a non-consistent performance of methods in com-

*Corresponding author

Email addresses: joonas.j.lahtinen@tuni.fi (Joonas Lahtinen , alexandra.koulouri@tuni.fi (Alexandra Koulouri), stefan.ramm@gmail.com (Stefan Ramm), joerg.wellmer@kk-bochum.de (Jörg Wellmer), carsten.wolters@uni-muenster.de (Carsten Wolters), sampsa.porsiaainen@tuni.fi (Sampsa Porsiaainen)

parison studies (Kirsch et al., 2006; de Gooijer-van de Groep et al., 2013; Hall et al., 2018; Neugebauer et al., 2022). Sometimes concordance of different source localization estimates can be linked with the Engel 1 outcome (Rampp et al., 2019; Li et al., 2021). The commendability of a method is usually measured in concordance between the resection area and reconstruction or score map, meaning overlap or partial overlap between a value peak produced by localization estimator and resection volume in lobar level (Kirsch et al., 2006; de Gooijer-van de Groep et al., 2013; Hall et al., 2018; Coito et al., 2019). Nevertheless, the definition of concordance varies between studies (Mouthaan et al., 2019) and it can be a gracious measure of the estimation accuracy since it is not necessarily clear what proportion of reconstruction is counted as the peak. Especially, the overlap of a widespread and blur reconstruction peak, as in the case of Standardized low-resolution brain electromagnetic tomography (sLORETA) (Hauk et al., 2011), can be misleading in such a context.

In ES location estimation, the most common approach is to use a single dipole fitting, also called single equivalent current dipole fitting, (Baumgartner et al., 2000; Otsubo et al., 2001; Knowlton et al., 2006), where the estimated location of the activity is defined to be the source point with the greatest goodness of fit (GoF) (Fuchs et al., 1998). In the study of Hall et al., the estimated candidate location with a GoF of more than 70% has been seen as reliable enough for further clinical evaluation (Hall et al., 2018). However, the dipole fitting approach is highly sensitive to signal-to-noise (SNR) ratio (Sekihara et al., 1996; Sakuma et al., 1999; Scherg et al., 2002). Moreover, dipole fitting can be seen to be overly simplistic to model complex electrical phenomena such as epileptic activity (Alarcón et al., 1999; Shiraishi et al., 2005). Indeed, the dipolar fitting is highly dependent on the applied forward model and with regard to neural activity as well as other factors such as the conductivity values of the scalp, skull, and different brain tissues (Vorwerk et al., 2019). In distributed modelling, not only dipolar activity can be recovered, but extended source configurations can be reconstructed too (Plummer et al., 2008). With those distributional methods, which are classified as hierarchical Bayesian methods (HBMs) (Calvetti et al., 2009), the properties of the brain's activity distribution are determined according to prior assumptions. Suitably chosen priors can improve the prediction power of a source estimation method. Another benefit of HBM is that the noise can be appropriately taken into account in the modelling scheme leading to stable estimations which have been demonstrated, for example, in the non-invasive recovery of weak subcortical brain activity using sparsity priors (Krishnaswamy et al., 2017; Rezaei et al., 2021; Sohrabpour and He, 2021).

In this study, we introduce a new robust methodology to estimate the location of interictal epileptic discharges in focal epilepsy with the goal to localize underlying epileptic sources. Our work is motivated by the current density standardization technique of Standardized low-resolution brain electromagnetic tomography (sLORETA) (Pascual-Marqui,

2002), the success of sLORETA in localization of ESs (Leal et al., 2008; de Gooijer-van de Groep et al., 2013; Coito et al., 2019), and employment of standardization with FOCUSS method (Liu et al., 2005). The standardization utilizes the resolution matrix of the lead field to ensure unbiased and correct localization estimation in a noiseless case when one source needs to be recovered (Sekihara et al., 2005; Greenblatt et al., 2005; Pascual-Marqui, 2007). Even when the measurement data is noisy, sLORETA has shown to be robust (Saha et al., 2015; Dümpelmann et al., 2012), i.e., the measurement noise can perturb the estimation only slightly, which is a relevant feature for ES localization. Moreover, sLORETA outperformed depth-weighted minimum norm estimate (wMNE) in a comprehensive simulated study (Grech et al., 2008), and standard methods with statistical parametrization have been shown to localize deep brain activity while wMNE mislocalizes (Attal and Schwartz, 2013). In a recent study of epilepsy source reconstruction via high-density EEG, sLORETA estimates epilepsy sources significantly smaller distances to resection volumes than wME (van de Velden et al., 2023). These findings further motivated us to focus on statistical standardization and normalization instead of depth-weighting. Standardization is a post-hoc weighting of the solution obtained from a linear or linearized localization algorithm to obtain a solution that is free from lead field-induced bias. As a demonstration of that, Standardized FOCUSS, referred to as Standardized Shrinking LORETA-FOCUSS (SSLOFO), can estimate the location of brain activity better than its basic counterpart (Liu et al., 2005) and it has been successfully used to reconstruct the P300 generator of event-related potentials aligning with functional neuroimaging studies (Schimpf and Liu, 2008). The development and theoretical research of standardization-type post-weighting methods has recently attracted interest in other inversion areas as well (Elvetun and Nielsen, 2021). These observations motivated us to couple the standardization with a recently introduced HBM that has conditionally exponential prior and has been shown to localize cortical and sub-cortical activity simultaneously with a high measurement noise robustness in numerical cases (Lahtinen et al., 2022) to investigate whether similar reconstruction improvements can be obtained as with the standardization of Minimum norm estimate and FOCUSS. Utilizing the Bayesian framework allows us to have freedom in the prior designs that affect the properties of the estimation, potentially enabling a more realistic solution. The investigated HBM has a prior parameter for adjusting the focality of the solution. The aim of coupling these methodologies is, first, to verify through simulations that the combined method is robust to additional measurement noise and examine what happens to the prior-based focality in the presence of standardization. Then, validate the method's ability to localize the focal epileptic source in patients.

We hypothesize that the epileptic activity can be explained best by a focal solver because, at the onset of a spike in focal epilepsy, one would assume a circumscribed generator. Otherwise, epilepsy surgery may not be viable. In this pa-

per, the method is called by its algorithmic name, *Hierarchical Adaptive Lp Regression* (HALpR), and the standardized counterpart as *Standardized Hierarchical Adaptive Lp Regression* (SHALpR). We analyze the effect of the standardization with simulated data of focal reference sources and real presurgical epilepsy data using head models constructed from MRI-data of two patients. Both of the patients underwent surgery and were seizure-free during the follow-up period that lasted more than four years. Standardized hierarchical methods are compared with their non-standardized counterparts and the noise-normalized dynamic statistical parametric map (dSPM) (Dale et al., 2000). Similar to standardized methods, dSPM aims to compensate for the depth bias with its own post-hoc weighting (Lin et al., 2006). dSPM, SSLOFO, and sLORETA are investigated as alternative distributional methods utilizing statistical parameterization that can be classified as HBMs (Wipf and Nagarajan, 2009). Hence, the purpose of this study partly includes the investigation of localization improvement of HBM when standardization is applied. For the sake of clarity and concrete results, we use the numerical Euclidean distance between the location of the reconstruction maximum and the boundary of the surgical resection volume. The precision of the measure is assured by patients' small epileptogenic lesions due to focal cortical dysplasia (Wellmer, 2018), prompted by the small size of the resection volumes, see sub-section 3.1.

Our results suggest that (1) the standardization improves the localization and noise robustness of the hierarchical Bayesian inverse method with both of the examined major prior degrees 1 and 2 corresponding to $L1$ - and $L2$ -penalization (HAL1R/HAL2R), respectively and that (2) SHAL1R can localize the activity inside the resection area within 1 cm accuracy more often than any other method with both numerically simulated and patient data.

2. Methodologies

The source estimation problem can be considered as a task to solve the ill-posed linear equation

$$\mathbf{y} = \mathbf{L}\mathbf{x} + \mathbf{n}, \quad (1)$$

where the vector $\mathbf{y} \in \mathbb{R}^m$ represents measurement data, $\mathbf{L} \in \mathbb{R}^{m \times n}$ is the lead field matrix, \mathbf{n} is Gaussian distributed measurement noise, and $\mathbf{x} \in \mathbb{R}^n$ is the brain activity to be reconstructed. The model dimension m indicates the number of measurement sensors and n is the number of sources (calculation nodes) in the source space multiplied by the orientational degrees of freedom.

We have used the Zeffiro Interface (ZI) toolbox for electromagnetic brain imaging (He et al., 2019) to calculate the lead fields. The forward model produced via ZI utilizes the finite element method (FEM) and the current conservation-based H(div) approach (Pursiainen et al., 2016; Bauer et al., 2015; Miinalainen et al., 2019). The finite element mesh was constructed from $T1$ -weighted MRI sequences. The segmentation of the brain volumes was performed using FreeSurfer

software¹ and subcortical structures were extracted from FreeSurfer's Aseg atlas. The finite element (FE) mesh of patients' heads was created with 1 mm resolution. The head model is based on a multi-compartment conductivity distribution composed of altogether 18 different cortical and subcortical segments. The conductivity values were selected following Dannhauer et al. (2011), associating the conductivity of the subcortical nuclei as e.g. in Rezaei et al. (2021) and Lahtinen et al. (2022). The conductivities are presented in Table 1. Anatomy has been taken into account as a hard constraint, meaning that there are no epileptic sources in the white matter.

Tissue	Value (S/m)
scalp	0.43
skull	0.0064
cerebrospinal fluid	1.79
white matter	0.14
grey matter	0.33
sub-cortical structures	0.33

Table 1: Conductivity values of used compartments in the forward model. The values are based on the study of Dannhauer et al. (Dannhauer et al., 2011).

To reconstruct the distributed current density or simply localize the brain activity, one needs to select an inversion algorithm for the task. Each method is based on specific *a priori* assumptions about the nature of brain activity. Next, we introduce the inversion methods investigated in this study.

2.1. Dynamic statistical parametric maps (dSPM)

Statistical parametric maps are methods to make inferences about regional effects (Flandin and Friston, 2019). In the case of dynamical statistical parametric mapping, the statistical scores for every source point $i = 1, \dots, n$ are obtained by noise-normalizing the dipole strength

$$z_i = \frac{\mathbf{e}_i^T \mathbf{L}^\dagger \mathbf{y}}{\sqrt{\mathbf{e}_i^T \mathbf{L}^\dagger \mathbf{C} (\mathbf{L}^\dagger)^T \mathbf{e}_i}}, \quad (2)$$

where \mathbf{e}_i is i th unit basis vector, $\mathbf{L}^\dagger = \mathbf{P} \mathbf{L}^T (\mathbf{L} \mathbf{P} \mathbf{L}^T + \mathbf{C})^{-1}$, $\mathbf{P} \in \mathbb{R}^{n \times n}$ is the source covariance and $\mathbf{C} \in \mathbb{R}^{m \times m}$ is the measurement noise covariance. These statistical parameters are by definition t -distributed under the null hypothesis of no dipolar activity at the i th source location (Dale et al., 2000).

2.2. Standardized low-resolution brain electromagnetic tomography (sLORETA)

sLORETA is a standardized minimum norm estimation (MNE) approach, where the MNE estimate (Hämäläinen and Ilmoniemi, 1994) is weighted by the diagonal or block diagonal elements of the resolution matrix \mathbf{R} corresponding to the MNE problem (Pascual-Marqui, 2002). The resolution matrix or point spread function is a linear map between the true

¹<https://surfer.nmr.mgh.harvard.edu/>

$\mathbf{x}^{(\text{true})}$ and estimated $\mathbf{x}^{(\text{est})}$ reconstruction under the assumptions that the linearized model L is correct and the random variables are distributed as $\mathbf{y} \mid \mathbf{x}^{(\text{true})} \sim \mathcal{N}(L\mathbf{x}^{(\text{true})}, C)$ and $\mathbf{x}^{(\text{true})} \sim \mathcal{N}(\mathbf{0}, P)$, where $C \in \mathbb{R}^{m \times m}$ is measurement noise covariance and $P \in \mathbb{R}^{n \times n}$ is the prior covariance matrix, i.e.,

$$\mathbf{x}^{(\text{est})} = PL^T (LPL^T + C)^{-1} L\mathbf{x}^{(\text{true})} = R\mathbf{x}^{(\text{true})}, \quad (3)$$

when MNE and sLORETA are interpreted within the Bayesian framework (Wipf and Nagarajan, 2009). The standardized estimation can be written as the power of source estimation using the inverse of diagonal blocks of the resolution matrix,

$$(\mathbf{x}_I^{(\text{est})})^T R_{II}^{-1} \mathbf{x}_I^{(\text{est})}, \quad (4)$$

where index set I represents the vector indices corresponding to a source location. The dimension of the set I depends on the number of orientational degrees of freedom on a dipole.

2.3. Standardized Shrinking LORETA-FOCUSS (SSLOFO)

Aiming at a method that combines the localization accuracy of sLORETA with the sparsity of FOCUSS, Liu et al. proposed *standardized FOCUSS* (Liu et al., 2005). The approach differs from the FOCUSS's iterations by updating the resolution matrix on each step as follows:

$$R^{(k+1)} = P^{(k)} L^T (LP^{(k)} L^T + C)^{-1} L, \quad (5)$$

where the prior covariance $P^{(k)} = W^{(k)}(W^{(k)})^T$ with

$$W^{(k)} = \text{Diag} \left(\left(\|L_{:,1}\|^{-1}, \dots, \|L_{:,n}\|^{-1} \right) \right) \times W^{(k-1)} \text{Diag} \left(\left(|x_1^{(k-1)}|, \dots, |x_n^{(k-1)}| \right) \right). \quad (6)$$

Shrinking of the reconstructed current distribution is achieved by first average smoothing the reconstruction $\mathbf{x}^{(k)}$ over a given range and excluding those source locations where the estimated current density amplitude is smaller than p percents of the estimated maximum current density amplitude. The algorithm is given in [Appendix A](#).

2.4. Hierarchical Adaptive L_p Regularization (HALpR)

Formulation of an inverse method using a hierarchical Bayesian model (HBM) allows us to examine the brain activity distribution statistically and to explain the given prior assumptions in a probabilistic form as a prior distribution. This article contemplates the HBM based on a Gaussian likelihood, conditionally exponential prior, and Gamma hyperprior, thus giving us the posterior distribution

$$p(\mathbf{x}, \boldsymbol{\gamma} \mid \mathbf{y}) \propto \exp \left(-\frac{1}{2} (\mathbf{Lx} - \mathbf{y})^T C^{-1} (\mathbf{Lx} - \mathbf{y}) \right) \times \exp \left(-\|\text{Diag}(\boldsymbol{\gamma})^{1/p} \mathbf{x}\|_p^p \right) \text{Ga}(\boldsymbol{\gamma}, \kappa, \theta), \quad (7)$$

where C is a noise covariance matrix, $\boldsymbol{\gamma}$ is a hyperparameter vector, κ is the shape parameter, θ is the scale parameter, and p is called the *prior degree* which is used for determine the sparsity of the prior (Lahtinen et al., 2022). A reconstruction

of the brain activity is obtained by evaluating the maximum a posteriori (MAP) estimate. On one hand, if one selects $p = 2$, the algorithm resembles MNE with reweighted regularization (Daubechies et al., 2010) in which fixed-point iteration attempts to gradually improve the regularization, according to Calvetti et al. (2009), which is computationally rather light. On the other hand, in a case where $p \neq 2$ we face a mixed-norm minimization problem for which many algorithms have been developed (Haufe et al., 2008). However, in a high-resolution FEM modelling scheme, the dimension of the problem is high, and, therefore, the computational burden can often be too much. For that reason, we perform fixed-point iterations with a Gaussian prior density that approximates the exponential prior that is shown to converge to $L1$ regularized solution (Calvetti et al., 2019). In that way, we can obtain the reconstruction via a linear mapping. The fixed-point iteration is continued until the duality gap reaches a certain tolerance. The stopping criterion for the duality gap approach is described in [Appendix C.1](#). Because the estimate is obtained as a tuple $(\mathbf{x}, \boldsymbol{\gamma})$, we need to use a sequential algorithm to update both variables. In this study, we use the Iterative alternating sequential (IAS) algorithm for updating the hyperparameter $\boldsymbol{\gamma}$ (Calvetti et al., 2009, 2020).

2.5. Standardization of Hierarchical Adaptive L_p Regularization (SHALpR)

Here we view standardization as a technique to transform the recovered parameters to statistical scores that are free from the lead field-induced localization bias when the task is to localize a single source. From this point of view, there are no restrictions for the applied linear inverse model.

To employ the standardization with the HBM, we use an approach similar to SSLOFO, resulting in the following updating rules for IAS iteration

$$\begin{aligned} \gamma_i^{(k)} &= \frac{\kappa + 1/p - 1}{|x_i^{(k)}|^p + \theta} \quad \text{for } i = 1, \dots, n, \\ \mathbf{x}^{(k+1)} &= \arg \min_{\mathbf{x}} \left\{ \frac{1}{2} (\mathbf{Lx} - \mathbf{y})^T C^{-1} (\mathbf{Lx} - \mathbf{y}) + \sum_{i=1}^n \gamma_i^{(k)} |x_i|^p \right\}, \\ P^{(k)} &= \frac{1}{2} \text{Diag} \left(\left(|x_1^{(k+1)}|^{2-p} / \gamma_1^{(k)}, \dots, |x_n^{(k+1)}|^{2-p} / \gamma_n^{(k)} \right) \right), \\ R^{(k+1)} &= P^{(k)} L^T (LP^{(k)} L^T + C)^{-1} L, \\ \mathbf{z}_I^{(k+1)} &= (R_{II}^{(k+1)})^{-1/2} \mathbf{x}_I^{(k+1)}. \end{aligned} \quad (8)$$

The derivation of the formulation is presented in [Appendix B](#). We have decided to use the matrix square root as the decomposition method for block-diagonal matrix R_{II}^{-1} , as advised in Pascual-Marqui (2007), to obtain \mathbf{z} because the matrix is not necessarily positive semi-definite if the number of dimensions is greater than one. By allowing the vector representation for the standardized final estimation, then the direction of the dipole vectors can also be estimated if necessary. The whole inversion algorithm is presented in [Appendix C](#).

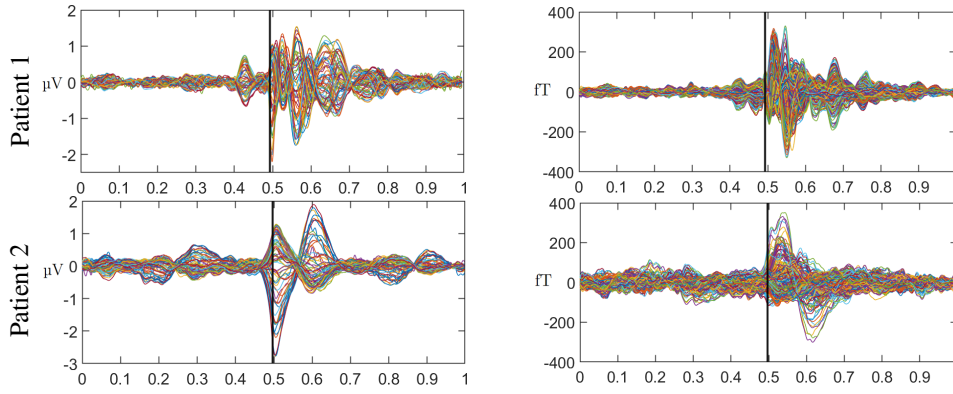


Figure 1: Butterfly plot of EEG (left) and MEG (right) recordings. The vertical line shows the rising flank as the picked epoch for reconstruction. The time point is chosen to balance the signal-to-noise ratio and the focality of the source, which weakens over time as the epileptic activity spreads in the brain structure.

3. Experimental data and simulations

The experiments conducted focused on reconstructing the activity generated in the resection revealing the source of focal epilepsy. The following sections give the patient descriptions, the observed non-invasive data with its pre-processing, and experiments with the real data and simulations in more detail.

3.1. Patient profiles

Patient 1 was 29 years old at the time of the EEG and MEG measurements. She suffered from pharmaco-resistant epilepsy. Her semiology was a somatosensory aura of the left arm followed by tonic-clonic movements of the left arm and hand. Data were evaluated and 248 interictal spikes were marked by a board-certified epileptologist based on non-invasive measurements. MRI measurements revealed focal cortical dysplasia (FCD) IIb of 1.2 cm³ lesional volume at the bottom of the sulcus according to high-resolution 3D-FLAIR (Fluid Attenuation Inversion Recover) and ZOOMit in the right superior parietal lobule. It was confirmed as a potential epileptic source by EEG and MEG source analysis of the marked spikes. The lesion and surrounding tissue (about 8 cm³) were surgically removed in February 2018. The patient was seizure-free for four years and the last follow-up took place in 2022.

Patient 2 was 17 years old at the time of EEG and MEG measurements. He had refractory seizures out of sleep, including vocalization followed by right-sided head version, asymmetrical tonic stiffening with right arm extension, and generalized tonic-clonic seizures. A small (about 0.4 cm³) FCD type IIb lesion was suspected in the anterior part of the left superior frontal sulcus on MRI based on PET (positron emission tomography) and EEG/MEG source analysis elicited from 54 marked spikes. Intracranial stereo-EEG recordings with six depth electrodes implanted in and around the MRI abnormality revealed interictal activity typical for a FCD with seizure onset from the abnormality. The patient was subsequently treated with stereotactically guided radiofrequency thermoablation in August 2017 (Wellmer et al., 2016), coagulating about 1.4 cm³. The patient was seizure-free for six years and the last follow-up took place in 2022.

The study was conducted according to the guidelines of the Declaration of Helsinki. Both subjects of this study have given informed consent.

3.2. Clinical EEG and MEG data

A standard EEG system of 74 channels including basal channels and common average reference was used for both patients. EEG electrode positions were digitized using a Polhemus digitizer (FASTRAK, Polhemus Incorporated, Colchester, VT). The MEG system (CTF Omega 2005 MEG by CTF, <https://www.ctf.com/>, last accessed on 26.10.2023) had 275 gradiometers, 4 of which were defective, and 29 reference sensors. Non-working channels were excluded when observed. The interference of magnetic fields caused by distant locations was reduced using the MEG reference coils to calculate first-order synthetic gradiometers. During the acquisition, the head position inside the MEG was tracked via three head localization coils placed on the nasion, left, and right distal outer ear canal. To get the best concordance with the MRI, the measurements were performed in the supine position, the patients were also measured in the supine position inside the MEG to reduce head movements and to prevent cerebrospinal fluid effects due to a brain shift when combining EEG/MEG and MRI (Rice et al., 2013). The data were measured with a sampling rate of 2400 Hz.

3.3. Data pre-processing

The epileptic spike data was pre-processed using Field-Trip (Oostenveld et al., 2011). The data was filtered using a two-pass zero-phase Butterworth Infinite Impulse Response Convolution (IIRC) filter of sixth order, where the high-pass was 2 Hz, the low-pass 80 Hz, and a notch filter was 50 Hz. Trials were created with 0.5 s of data before and after the peak of the spikes. These trials were checked for similar topographies and then averaged to improve the signal-to-noise ratio (SNR) of the interictal spike patterns.

On selection of the time epoch, one needs to balance between the uncertainty following the spike propagation and low signal strength on the spike onset. Thereby, the middle point of the rising flank has been recommended as the time

point for localization (Lantz et al., 2003) and hence used for the patient data. The selected time points are displayed as vertical lines over patients' EEG and MEG recordings in Figure 1.

3.4. Setup of the synthetic experiments

Using the goodness of fit (GoF) measure of the dipole scan

$$g_i = 1 - \frac{\|y - L_i L_i^+ y\|^2}{\|y\|^2}, \quad (9)$$

where L_i is the sub-lead field matrix of i th source location and $(\cdot)^+$ denotes pseudo-inverse, it seems that the EEG measurements could be modelled reasonably well by a single dipole: by having GoF scores 0.97 for Patient 1 and 0.85 for Patient 2 on the scale from 0 to 1. However, MEG measurements that describe essentially the same activity have GoF values of 0.66 and 0.36, respectively. Thereby, one could conclude that the activity cannot be explained as a point-like source particularly well (Hall et al., 2018; Neugebauer et al., 2022; Unnwongse et al., 2023). Hence, we use multiple Gaussian blurred sources to simulate the epileptic activity. Blurring also partly prevents us from reinforcing the assumptions behind the forward model, i.e., moving us further away from an inverse crime.

For the first experiment setup, we aim to create synthetic EEG and MEG data that simulates as well as possible to the epilepsy measurements of both patients and that originate from a source configuration that is smoothly distributed in the resection volumes. Smoothness can be achieved by Gaussian blurring of point sources and the similarity between the synthetic and measured data depends on the number of smoothed dipolar sources used in measurement modelling. First, we define the Gaussian blur matrix G that spreads the activity of each source position inside the resection area on neighboring source points. After that, we calculate the least absolute deviation between modelled and real measurement data, i.e., minimize $\|LG\mathbf{d} - \mathbf{y}\|_1$, with respect to \mathbf{d} . This way, vector $G\mathbf{d}$ gives us a data-describing blurred brain activity distribution where every calculation node inside the resection has a non-zero contribution to norm minimization including dipolar vectors that cancel each other out while projected to measurements due to the ill-posed nature of the system. To avoid the condition described above, we select 20 % of the dipoles from \mathbf{d} having the highest contribution in the norm minimization. Next, recalculate the minimization problem for the sub-system induced by the most fitting dipoles represented in \mathbf{d}_{sub} . The percentage is selected so that the relative error is less than 1 % for each case. In the end, the activity to be reconstructed is $G_{\text{sub}}\mathbf{d}_{\text{sub}}$. Reconstruction is obtained using previously presented methods HAL2R, HAL1R, SHAL2R, SHAL1R, SSLOFO, and sLORETA without filtering or altering the lead field through smoothing or other means.

That way, we decrease the number of redundant dipoles and avoid over-fitting. The signal-to-noise ratio is assumed to come from the fitting to actual noisy data, which is why

the simulated noise component is not added to this experiment. Figure 2 shows real and synthetic data side-by-side. To avoid an inverse crime, we have removed 30 % of randomly selected source points from the head models. The main point of the experiment is to verify that the reconstruction obtained using the measurement modeling scheme is in accordance with the results we get with real data. Therefore, this experiment serves as a validation for the following, second numerical experiment.

The location estimate is decided by the commonly used maximum principle which is a suggested approach with distributed methods like MNE and sLORETA (Hämäläinen and Ilmoniemi, 1994; Fuchs et al., 1999; Sekihara and Nagarajan, 2008; Samuelsson et al., 2021), meaning that we decide the location of reconstruction maximum to be the estimated location of the activity. According to (Pascual-Marqui, 2002), estimating the source by maximum component is the core principle for standardization as the recovered parameters of inversion are statistical scores assigned to each source point individually, not current density distributions. In this sense, it is similar to spatial filtering or dipole scanning with GoF measure but different in the sense that the stated inversion method like MNE, FOCUSS, or presented HBM allows the source to have an extended nature in which the center is evaluated via maximum principle.

Here we use the Euclidean distance from the location estimation to the nearest boundary of resection volume as the measure of the localization error. Additionally, we calculated the earth mover's distance (EMD) (Kantorovich, 1940; Vaserstein, 1969; Rubner et al., 1998) as a measure of reconstruction's spread outside the resection volume. The earth mover's distance describes the work needed to push the whole reconstruction inside the resection volume and match the shape of the true activity distribution (Lucka et al., 2012; Lahtinen et al., 2022).

In the second synthetic experiment, we aim to verify that the standardization applied to the studied HBM leads to noise robustness similar to the case of MNE. Additionally, we desire that the experiment setup would reflect the patients' epilepsy data as much as possible. For this reason, we use a single blurred dipole that best explains the data for 25 % of the sensors nearest to the resection area. This proportion of optimally selected subset of electrodes was found to increase the estimation accuracy compared to the full set of electrodes (Soler et al., 2022). In fact, the SNR is poor for channels far from the source of the activity, suggesting that appropriate channel reduction can increase the clarity of the activity we are seeking via reverse engineering. Moreover, principles of linear inversion imply that the polarity of the measurements does not affect the localization when the location estimation is determined by the maximum of the reconstruction magnitude. The reconstructed blurred dipolar activity is assumed to present a noiseless activity. To ensure a fair comparison, we use the same random number generator seed in generating an additional Gaussian noise for 50 samples used for each noise level and all methods. The SNR levels used are 30, 20, 10, and 5 dB. To investigate the sta-

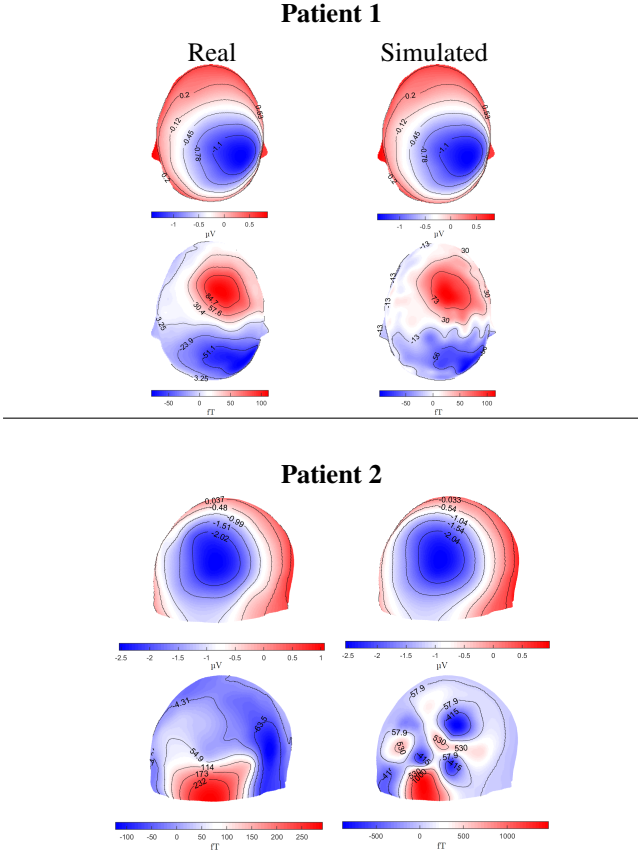


Figure 2: Patient measurements (left) and simulated measurements (right) of the epoch projected and interpolated on the scalp models. The first row of both sets presents EEG measurements and the second row displays MEG measurements.

tistical significance, we use the Siegel-Tukey test which is a non-parametric test for equal variability (Siegel and Tukey, 1960). In this case, we want to test does the standardization decreases the variability of the estimation error, i.e., whether it reduces the effect of randomized noise.

3.5. Localization result visualization

To visualize the reconstruction spreads in localization experiments with simulated and real data, we utilize the volumetric visualization of ZI providing images including skull, white and grey matter layers, and sub-cortical structures, e.g., brainstem, thalamus, and cerebellum. The white matter layer is presented with a white since no activity can be placed there for physiological reasons discussed at the beginning of Section 2. The reconstructions are visualized in three main cutting planes (transversal, coronal, and sagittal). Locations of the planes are set by the location of the maximum reconstruction magnitude. From the perspective of one orthogonal plane, the locations of the other two planes are shown with horizontal and vertical lines. Their intersection points to the maximum reconstruction point.

For visual clarity and to give a sense of the spread difference across the localization methods, the visual presentations of the reconstructions are thresholded to 70 % (about 3 dB) below the maximum strength following a trend set by

(Li et al., 2016) in their study of epilepsy source localization. The thresholding is not used as a post-processing technique in calculations of the metrics.

3.6. Inverse model parameters

Investigated HBMs and SSLOFO have parameters to be set by the user. To have a reliable picture of the effects of standardization, we set the parameters for non-standardized and standardized methods to be the same. With all HBM methods, we used 20 IAS iterations that have been shown to be sufficient for convergence (Lahtinen et al., 2022). Rezaei et al. have suggested a method for hyperparameter selection for HBM with conditionally Gaussian priors (Rezaei et al., 2020) that we utilize with HAL2R, SHAL2R, and sLORETA. Unfortunately, such an approach is not highly applicable with a method of mixed norms, therefore, (S)HAL1R hypermodel's parameters are selected via the selection method described in (Lahtinen et al., 2022). For SSLOFO, we have set the space reduction percentage to 10 % suggested by Liu et al. (Liu et al., 2005), and the smoothing radius is chosen to be 1 cm.

3.7. Supplementary material

In addition to the aforementioned analysis, a numerical experiment to reconstruct a deep (mesocortical) source in the posterior cingulate cortex was conducted (Supplementary Materials 1.1) together with a test using real data in which the source space was limited into the cerebral cortex omitting the cerebellar cortex and subcortical structures (Supplementary Materials 1.2) which, otherwise, were included in the active part of the domain. The results of these additional numerical experiments have been included as supplementary material of this study.

4. Results

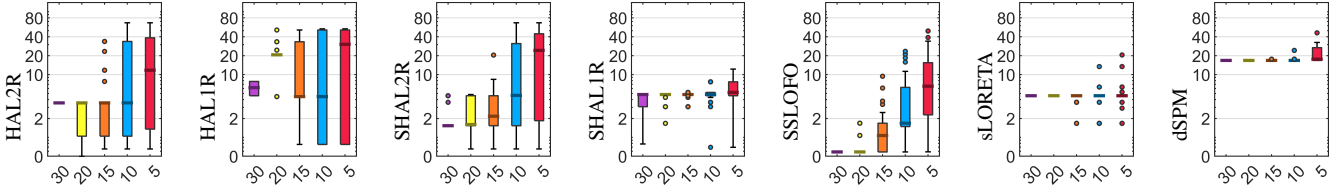
We have conducted an experiment to localize the epileptic source based on non-invasive EEG and MEG recordings using the resection area as the ground truth of location. Additionally, we simulated the epileptic activity on the resection area by blurring a dipolar point activity with a Gaussian convolution kernel to cover the whole area. Localization results obtained with selected inversion methods are consistent with the real and synthetic cases. We also conducted an experiment of multiple signal-to-noise ratios to verify that the standardization leads to more noise-robust localization for the studied HBM. Meaning, localization estimates vary less due to measurement noise and the increase of it.

4.1. Noise robustness experiment

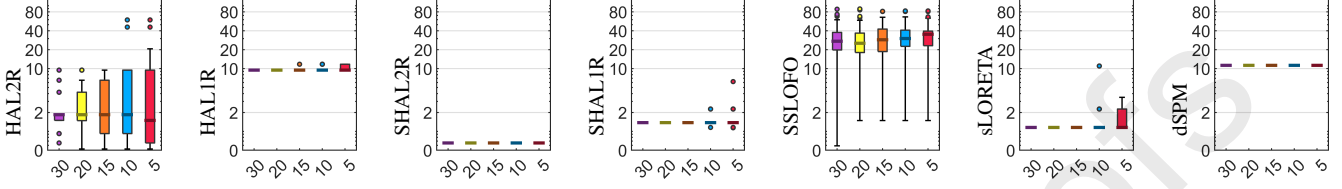
Increased robustness of HBMs after standardization is obtainable for both patients' resection volumes and both modalities in the box plots presented in Figure 3 achieving statistical significance examined with Siegel-Tukey test, see Table 2. Significant noise reduction can be seen in most of

Patient 1

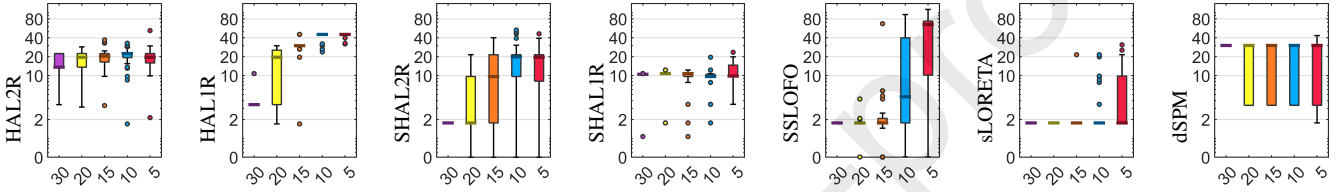
EEG



MEG

**Patient 2**

EEG



MEG

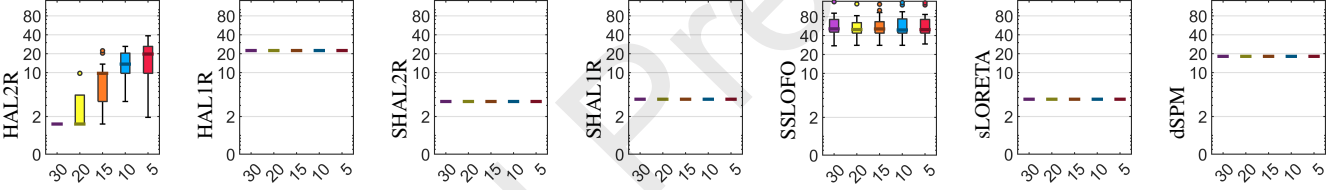


Figure 3: Results of the noise robustness test performed using simulated data generated using Gaussian blurred activity over the resection areas of two patients' head models. Localization error (y-axis), measured as the Euclidean distance from the boundary of the resection volumes, is displayed in millimeters. Signal-to-noise ratios (x-axis) are displayed in decibels. The thick line on the boxes indicates the median. Each data group with a certain signal-to-noise ratio contains 50 samples. Compared methods are (standardized) hierarchical adaptive L_p regression ((S)HALpR) for two penalty degrees L_1 and L_2 , standardized Shrinking LORETA-FOCUSS (SSLOFO), standardized low-resolution brain electromagnetic tomography (sLORETA), and dynamic statistical parametric maps (dSPM).

the experimented cases except S-/HAL2R comparison using Patient 1 head model at 15 dB SNR and lower, and S-/HAL1R comparison using Patient 2 head model at 15 and 5 dB both for EEG. Particularly, we can see that in the reduction of the interquartile range (size of colored boxes) comparing non-standardized HBMs HAL2R and HAL2R to their standardized counterparts SHAL2R and SHAL1R. The change in robustness is the most noticeable with L_2 -penalized HBM, HAL2R, using MEG data. However, the measurement noise robustness of the compared methods was deemed inferior compared to the basic sLORETA at the noise level of 5 dB. A similar effect can be obtained also for SSLOFO and dSPM. The median localization accuracies of the standardized HBMs, indicated by darker horizontal lines on boxes, are less than 1 cm in 10 dB and above for Patient 1. In the case of Patient 2, the same is true in 20 and 30 dB. Localization error of L_1 -penalized version is slightly above 1 cm. Non-standardized counterparts can have localization

errors less than 1 cm at high SNR levels but not consistently throughout the studied cases. MEG as the modeling scheme appears more favorable for non-standardized methods considering the accuracy and noise robustness. With EEG data, SSLOFO demonstrates comparably high localization accuracy with 15 dB or greater SNR, while for 10 dB or lower SNR, the results deteriorated. On the other hand, the method exhibits an error larger than 3 cm in 154 cases out of 300 for the Patient 1 model and 288 out of 300 for the Patient 2 model with MEG data all SNR levels combined. The basic sLORETA and dSPM have the highest noise robustness of all the methods compared. Regardless, localization accuracy of dSPM is mostly on the same level as non-standardized HAL1R, and sLORETA is able to produce significant mislocalizations as outliers, indicated as individual dots, starting from 15 dB in the case of simulated Patient 2 EEG.

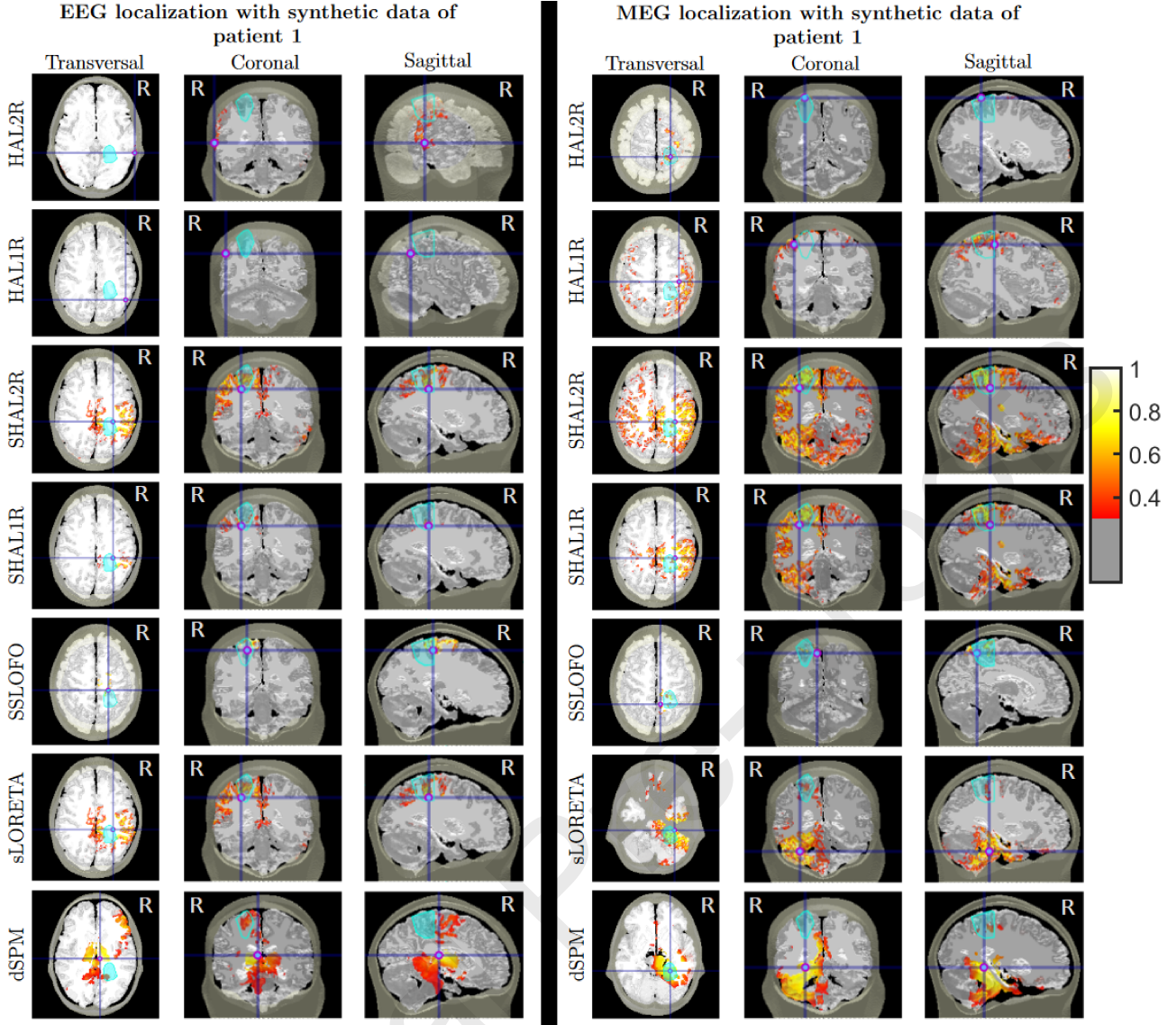


Figure 4: Highest 70 % of reconstructed source strengths and reconstruction maximum-based localization estimates for simulated Patient 1 data visualized on the main orthogonal planes of the volumetric head model. The dot marker indicates the location estimation and the vertical and horizontal lines represent the placement of the other two cut planes. The resection area is displayed in turquoise color. Turquoise borders are visible in each plane to indicate the location of the resection. Reconstructions are normalized such that the value 1 indicates the highest estimated magnitude. The color bar on the right shows the color-value correspondence and the threshold. The names of the cut planes are displayed on the top of the image columns and the name of the method corresponding to each row is shown on the left. Labels L/R indicate the anatomical left and right of the patient. In sagittal views, L and R represent the displayed hemisphere. The hemisphere is chosen by the estimated location. Compared methods are (standardized) hierarchical adaptive L_p regression ((S)HALpR) for two penalty degrees L_1 and L_2 , standardized Shrinking LORETA-FOCUSS (SSLOFO), standardized low-resolution brain electromagnetic tomography (sLORETA), and dynamic statistical parametric maps (dSPM).

4.2. Simulated localization experiment

In EEG source localization (left column on Figures 4 and 5), methods' localization accuracy varies between 1 mm to 4.5 cm for synthetic data. Only SHAL1R and sLORETA of the methods compared have localization accuracy that is consistently less than 1 cm, as shown in Table 3. Moreover, SHAL1R and sLORETA localization estimate points mainly on the same mesh node.

In the left-hand side of Figure 4, SHAL2R and sLORETA reconstructions of the synthetic Patient 1 EEG epoch extend between superior frontal lobes and reach sub-cortical areas.

Whereas the reconstruction via SSLOFO extends slightly towards the central gyrus. dSPM reconstruction peak is located at the thalamus and extends over the region of true activity. HAL1R and HAL2R point falsely to the right temporal lobe. MEG reconstruction of SHAL1R, SHAL2R, and sLORETA formed false activity concentration extending on the cerebellum and brainstem. Unlike SHALpRs, sLORETA does not recover the actual location of the activity at all. SSLOFO produced focal reconstruction about 2 cm away from the resection towards the longitudinal fissure. dSPM have a widespread reconstruction over the right

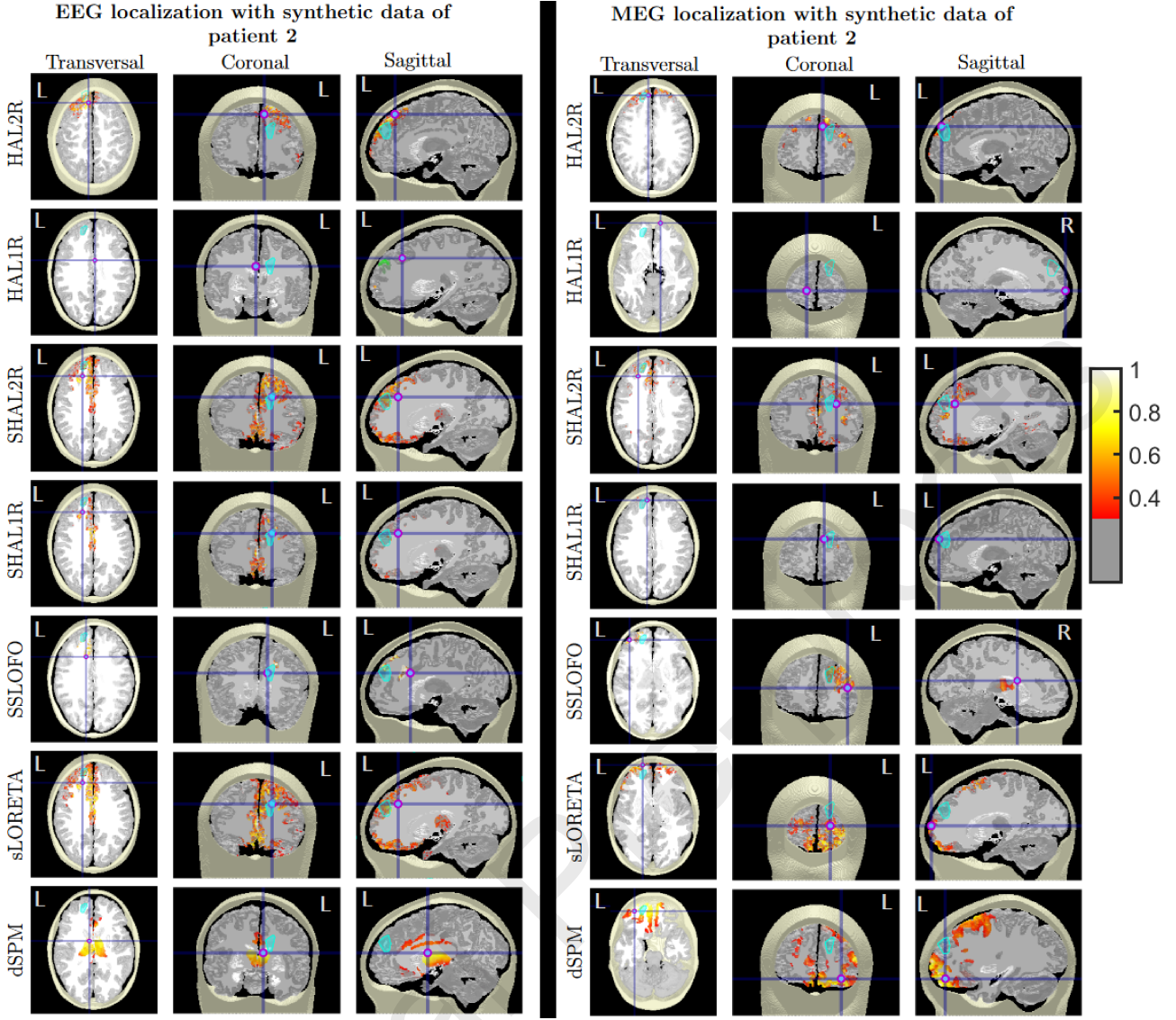


Figure 5: Highest 70 % of reconstructed source strengths and reconstruction maximum-based localization estimates for simulated Patient 2 data visualized on the main orthogonal planes of the volumetric head model. The dot marker indicates the location estimation and the vertical and horizontal lines represent the placement of the other two cut planes. The resection area is displayed in turquoise color. Turquoise borders are visible in each plane to indicate the location of the resection. Reconstructions are normalized such that the value 1 indicates the highest estimated magnitude. The color bar on the right shows the color-value correspondence and the threshold. The names of the cut planes are displayed on the top of the image columns and the name of the method corresponding to each row is shown on the left. Labels L/R indicate the anatomical left and right of the patient. In sagittal views, L and R represent the displayed hemisphere. The hemisphere is chosen by the estimated location. Compared methods are (standardized) hierarchical adaptive L_p regression ((S)HALpR) for two penalty degrees L_1 and L_2 , standardized Shrinking LORETA-FOCUSS (SSLOFO), standardized low-resolution brain electromagnetic tomography (sLORETA), and dynamic statistical parametric maps (dSPM).

cerebellum, reaching the bottom of the temporal lobe and the longitudinal fissure. In contrast to EEG, the activity localization of non-standardized HAL1R and HAL2R are less than 1 cm when reconstructing using MEG data (right-hand side of Figure 4). Both HBMs reconstructions gained spread when the standardization was applied to them. Considering Patient 2 in Figure 5, most EEG reconstructions extend between the superior frontal lobes, except dSPM which shows activity on the thalamic area and cingulate cortex. The superior frontal lobe extension can be obtained in sLORETA and SHAL2R for MEG. Localization estimations of HAL1R and sLORETA are further on the anterior than the resection

and the SSLOFO and dSPM estimates are too much on the lateral, see right-hand side of Figure 5.

Considering earth mover's distances in Table 3, SSLOFO has the smallest spread due to its source space shrinkage procedure. Comparing standardized HBMs to sLORETA, HBMs have generally smaller earth mover's distances even in cases where the localization is better for sLORETA. EMD for dSPM is the largest almost in every case except Patient 1 MEG, where sLORETA has the largest value.

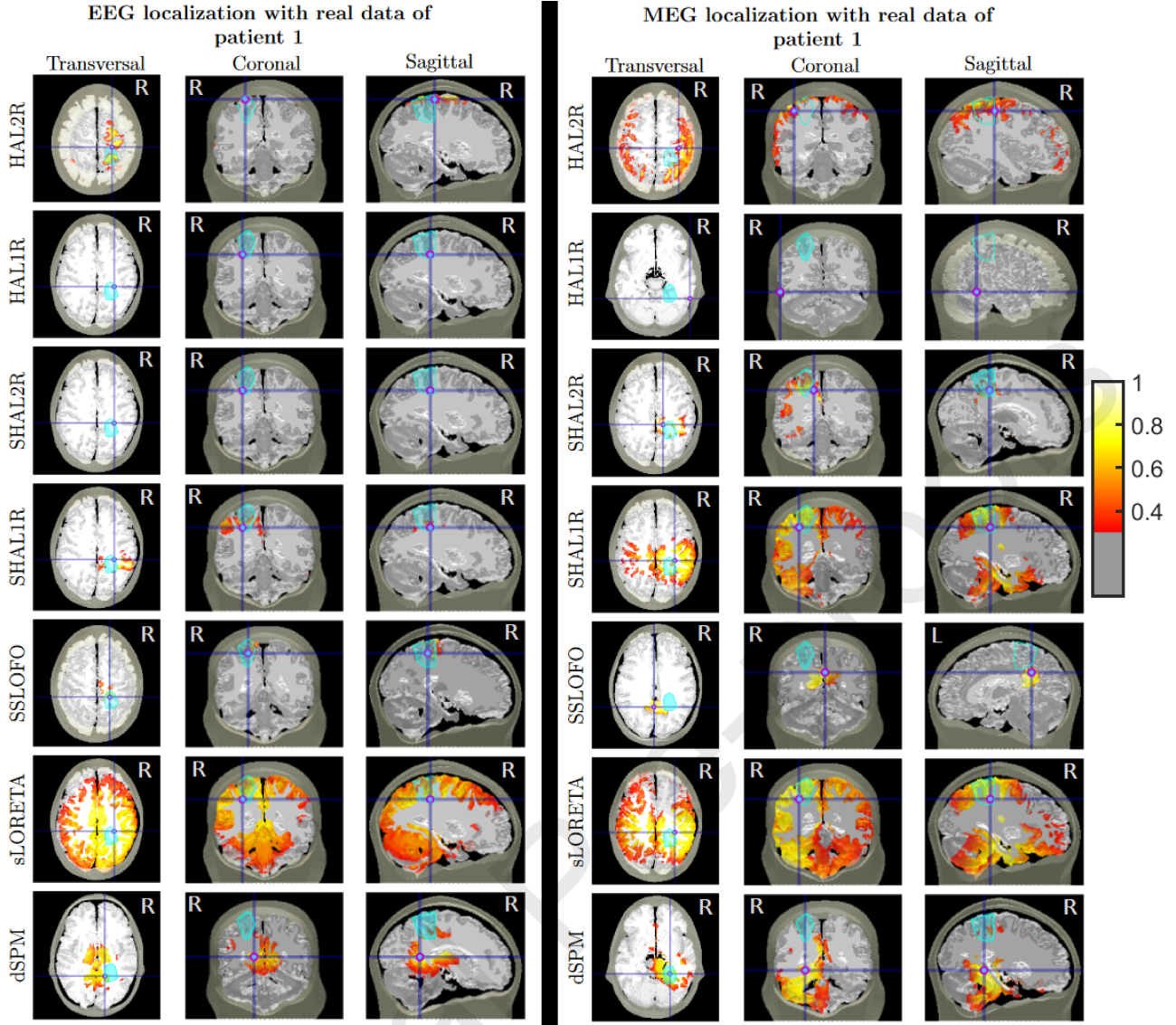


Figure 6: Highest 70 % of reconstructed source strengths and reconstruction maximum-based localization estimates for the measured Patient 1 epilepsy data visualized on the main orthogonal planes of the volumetric head model. The dot marker indicates the location estimation and the vertical and horizontal lines represent the placement of the other two cut planes. The resection area is displayed in turquoise color. Turquoise borders are visible in each plane to indicate the location of the resection. Reconstructions are normalized such that the value 1 indicates the highest estimated magnitude. The color bar on the right shows the color-value correspondence and the threshold. The names of the cut planes are displayed on the top of the image columns and the name of the method corresponding to each row is shown on the left. Labels L/R indicate the anatomical left and right of the patient. In sagittal views, L and R represent the displayed hemisphere. The hemisphere is chosen by the estimated location. Compared methods are (standardized) hierarchical adaptive L_p regression ((S)HALpR) for two penalty degrees L_1 and L_2 , standardized Shrinking LORETA-FOCUSS (SSLOFO), standardized low-resolution brain electromagnetic tomography (sLORETA), and dynamic statistical parametric maps (dSPM).

4.3. Localization experiment with clinical data

In the case of Patient 1, SHAL1R, SHAL2R, and sLORETA provide consistent localization estimates for EEG and MEG (Figure 6). Reconstructions of EEG recordings exhibit focal activity while most MEG reconstructions present activity that extends to the opposite hemisphere, except HAL1R and HAL2R. Reconstructed EEG data of Patient 2 (the left-hand side of Figure 7) extends to the ventral areas near the hypothalamus in sLORETA and SHAL1R. Activity between superior frontal lobes is obtained with every method for EEG and with SHAL1R, SSLOFO, sLORETA, and dSPM for MEG, as shown in the right-hand side of

Figure 7. It is worth noting that activity extends of this kind are obtained in simulated cases, where the true activity is limited inside the resection volume. The focality of the L_2 -penalized HBM's reconstruction is better when standardization is applied, but a significant spread can be obtained for the standardized L_1 -penalized method (SHAL1R) which produces a focal estimation without standardization. Whereas sLORETA has the most spread reconstruction.

In Patient 2, the activity is not localized from real data as accurately as in synthetic cases, see Figures 5 and 7. Most MEG-based source localization estimates are concentrated in a small region including the Broca's area while SSLOFO

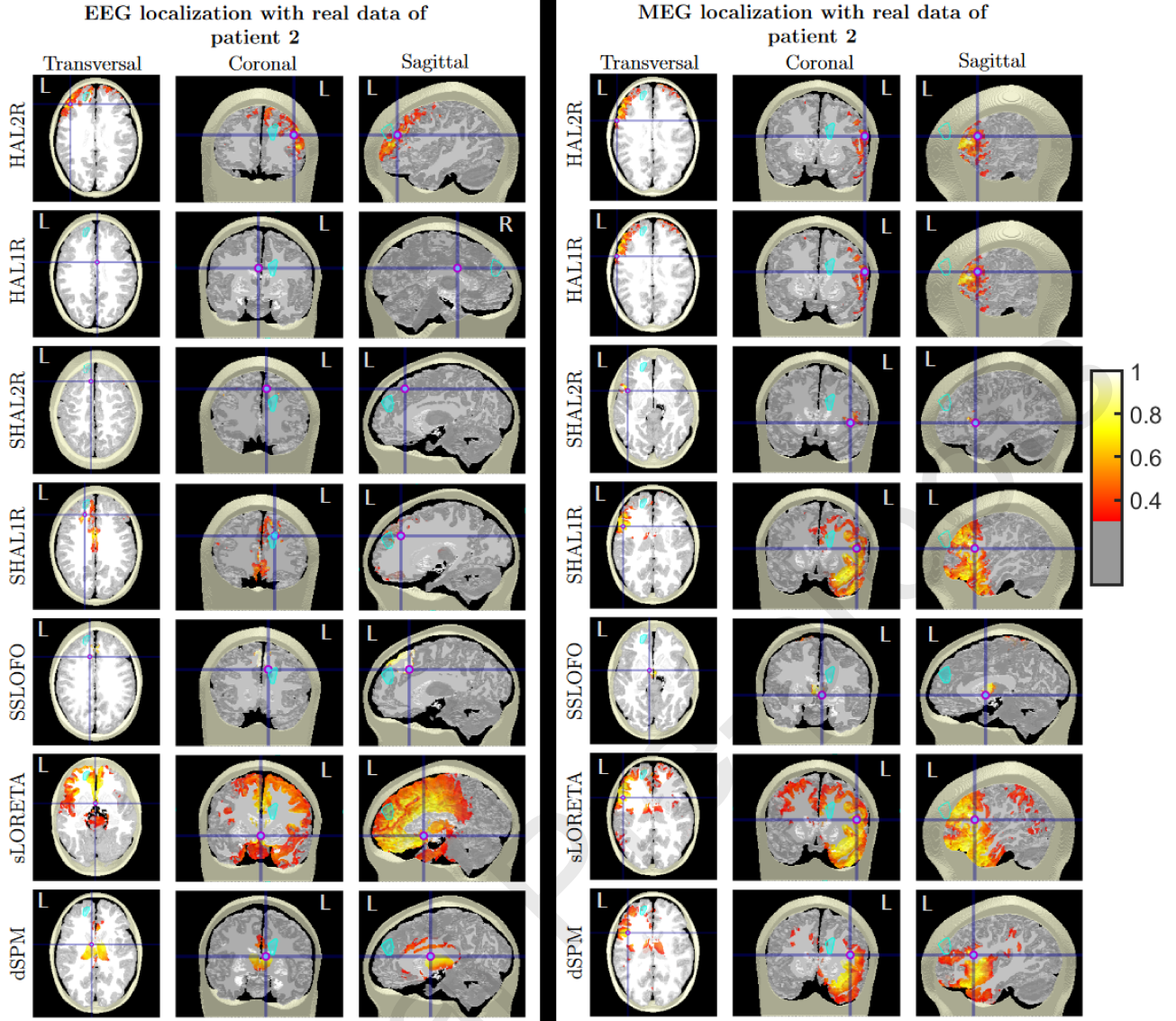


Figure 7: Highest 70 % of reconstructed source strengths and reconstruction maximum-based localization estimates for the measured Patient 2 epilepsy data visualized on the main orthogonal planes of the volumetric head model. The dot marker indicates the location estimation and the vertical and horizontal lines represent the placement of the other two cut planes. The resection area is displayed in turquoise color. Turquoise borders are visible in each plane to indicate the location of the resection. Reconstructions are normalized such that the value 1 indicates the highest estimated magnitude. The color bar on the right shows the color-value correspondence and the threshold. The names of the cut planes are displayed on the top of the image columns and the name of the method corresponding to each row is shown on the left. Labels L/R indicate the anatomical left and right of the patient. In sagittal views, L and R represent the displayed hemisphere. The hemisphere is chosen by the estimated location. Compared methods are (standardized) hierarchical adaptive L_p regression ((S)HALpR) for two penalty degrees L_1 and L_2 , standardized Shrinking LORETA-FOCUSS (SSLOFO), standardized low-resolution brain electromagnetic tomography (sLORETA), and dynamic statistical parametric maps (dSPM).

and dSPM estimates are almost in the center of the model. Considering the low goodness of fit (0.36) and the visual dissimilarity of the fitted multiple blurred sources (Figure 2), poor localization to the resection area is expected. With non-standardized HBMs, we obtained overall similar reconstructions. When standardization is applied to the methods, the reconstruction of SHAL1R has more similarities with sLORETA reconstruction than SHAL2R.

The localization of the brain activity for Patient 1 ended up being more consistent overall. Under one-centimeter localization accuracy was reached via HAL2R, standardized HBMs, and sLORETA for both EEG and MEG. HAL1R and

SSLOFO were able to localize the resection volume with EEG only, localization error being 2.0 and 0 mm, respectively. The greatest accuracy was obtained with standardized HAL1R and sLORETA with equally small distances to the resection volume, 2.0 mm for EEG and 2.8 mm for MEG. SHAL1R was the only method to localize the activity within 1 cm of the resection area in the case of Patient 2, but only based on EEG data. Basic and standardized HAL2R with SSLOFO have accuracy around 2 cm. Localization errors are displayed in Table 4.

Table 2: P-values given by Siegel-Tukey test for comparing measurement noise results of Hierarchical adaptive L_p regression and its standardization in Figure 3. $p < 0.05$ rejects the null hypothesis that both inversion results have the same variability. Shades represent the significance level as indicated in the table. Inconclusive cases where the localization error does not vary for either method are marked by \times . L1 and L2 on the leftmost column indicate the L_p degree of the regression compared.

Patient 1's head model					
SNR (dB):	30	20	15	10	5
EEG	L1				
	L2				
MEG	L1	\times	\times		
	L2				
Patient 2's head model					
EEG	L1				
	L2				
MEG	L1	\times	\times	\times	\times
	L2				

$p < 0.001$

$0.001 \leq p < 0.02$

$0.05 < p < 0.1$

5. Discussion

The standardization as a post-hoc weighting has two desirable qualities: enhanced localization accuracy and robustness to measurement noise (Saha et al., 2015; Dümpelmann et al., 2012; Neugebauer et al., 2022) obtained previously by standardizing MNE (Pascual-Marqui, 2002) and FOCUSS (Liu et al., 2005). In this study, we present the mathematically rigorous modus operandi to couple the standardization to the hierarchical Bayesian methods and apply it with the method utilizing exponential prior, where two of the major prior degrees were considered, resulting in L_2 and L_1 penalized minimization algorithms to find the reconstruction. The performance of the algorithms was investigated regarding the non-standardized versions, standardized FOCUSS, sLORETA, and dSPM. The last one is added as another post-hoc weighting scheme to reduce the depth bias to further motivate the decision to apply standardization instead of noise normalization. The results suggest that while noise normalization makes the estimation noise robust and reduces the depth bias, the localization is not as good as with standardization. The reason might be that as the standardization removes the lead field-induced bias in noiseless and theoretical settings (Sekihara and Nagarajan, 2008), dSPM is only claimed to compensate it (Hauk et al., 2011; Knösche and Haueisen, 2022). As a depth-weighting strategy, dSPM could just move the bias deeper from the vicinity of the model boundary.

In this study, we decided to construct our own numerical simulations to compare the EEG/MEG reconstruction methods and evaluate the effects of standardization instead of employing other custom-made validation procedures, e.g., Grova et al. (2006) that are limited to fixed forward models and fails to consider other noise generators than the one coming from the measurement device, e.g., a simultaneous and

spontaneous activity that could obscure the localization of a cortical epilepsy source.

We found that while 30 dB was the only SNR level where the estimates obtained via non-standardized counterparts HAL1R and HAL2R are not affected by the measurement noise, noise robustness is achieved in every examined noise level above 5 dB with both of the standardized HBMs called SHAL1R and SHAL2R, which is also the case with compared the standardized SLOFO. However, sLORETA was found to be noise robust even with the smallest experimented SNR in the simulated experiment. The localization accuracy with SHAL1R was found to be within 1 cm in every simulated localization experiment conducted. In the numerical experiment considering measurement noise levels from 5 to 30 dB, the previous was found to be true except for EEG in the noise level of 5 dB, which is, however, extremely poor signal-to-noise ratio. For SHAL2R, the results are also within 1 cm but inferior to those of sLORETA for EEG. In addition, considering the EMDs as a measure of reconstruction spread, SHAL1R has significantly smaller EMDs than sLORETA in almost all cases.

The results suggest that by using Laplace prior, i.e., L_1 penalized minimization problem, we can achieve the accuracy of sLORETA while maintaining some of the focality coming from the prior model when the estimates are standardized. The focal solution makes the location of the epileptic source easier to perceive based on the reconstruction map plotted over the brain tissue. Even if the localization of the reconstruction maxima is accurate for sLORETA, it is sensitive to all possible model uncertainties. Therefore, it is not advisable to use the maximum reconstructed value in the guidance of surgical decisions instead of the full distribution. Even if the usage of reconstruction to indicate the source location can be considered enough when the source is focal and because source localization is only one guiding tool out of many in presurgical workup routine (Rosenow and Lüders, 2001; Mouthaan et al., 2019; Neugebauer et al., 2022). A shortcoming of the standardization technique itself, as it is designed to reduce the bias defined by diagonal elements of a resolution matrix (Sekihara and Nagarajan, 2008), is that the approach is based on the underlying assumption of a single true source. Therefore, it can cause a significant mislocalization when multiple regions have strong activities as has been found in practical cases via sLORETA by Wagner et al. (2004); Mohd Zulkifly et al. (2022).

In light of our results, Standardized FOCUSS presents itself also as a considerable method for localizing epileptic activity using EEG when the noise level is not particularly low. However, the method seems to fail with experimented MEG data. The reason might be in the depth-balancing presented in formula (6) and the fact that the MEG signal, as it is modelled in the forward model, decays rapidly by depth leading the reconstruction maxima near the focus point of sensors that is in the middle of the model, i.e., near the thalamic area.

Applying the methods to the epilepsy data, we see similar behavior with simulated and real EEG data in which stan-

	HAL2R	HAL1R	SHAL2R	SHAL1R	SSLOFO	sLORETA	dSPM
Patient 1							
Dipole localization errors (mm)							
EEG	44.2	20.6	2.0	2.0	1.1	2.0	25.8
MEG	0.9	9.0	2.8	2.8	8.1	59.7	34.8
Earth mover's distances (mm)							
EEG	42.3	28.2	24.4	20.8	13.8	25.4	48.1
MEG	15.2	25.4	23.0	23.7	4.5	56.3	53.2
Patient 2							
Dipole localization errors (mm)							
EEG	16.4	45.2	9.7	9.7	24.4	9.7	48.0
MEG	4.4	34.7	7.8	2.3	21.5	17.2	33.8
Earth mover's distances (mm)							
EEG	30.9	44.8	31.3	35.9	12.5	30.5	55.7
MEG	22.6	39.8	21.0	14.5	11.7	36.7	48.6

Table 3: Dipole localization errors as Euclidean distance from the estimated location to the boundary of the resection volume and the earth mover's distances of reconstructions for synthetic EEG/MEG data. Both measures are in units of millimeters. Compared methods are (standardized) hierarchical adaptive L_p regression ((S)HALpR) for two penalty degrees L_1 and L_2 , standardized Shrinking LORETA-FOCUSS (SSLOFO), standardized low-resolution brain electromagnetic tomography (sLORETA), and dynamic statistical parametric maps (dSPM).

	HAL2R	HAL1R	SHAL2R	SHAL1R	SSLOFO	sLORETA	dSPM
Patient 1							
EEG	0.4	2.0	2.0	2.0	0	2.0	24.2
MEG	9.0	48.8	7.3	2.8	25.3	2.8	34.8
Patient 2							
EEG	22.4	45.2	20.7	9.7	21.6	47.5	48.0
MEG	52.1	52.1	43.7	44.0	49.5	44.0	37.8

Table 4: Dipole localization errors as Euclidean distance from the estimated location to the boundary of the resection volume for patients' EEG/MEG data. Both measures are in units of millimeters. Compared methods are (standardized) hierarchical adaptive L_p regression ((S)HALpR) for two penalty degrees L_1 and L_2 , standardized Shrinking LORETA-FOCUSS (SSLOFO), standardized low-resolution brain electromagnetic tomography (sLORETA), and dynamic statistical parametric maps (dSPM).

standardized HBMs localize almost on the boundary of the resection volume in both patients. However, deviance is observable with MEG reconstruction, more with Patient 2 than with Patient 1. It should be noted that the simulated and real datasets are notably different, indicating discrepancies between the actual head and its electromagnetic properties and the MEG forward model used. Moreover, we cannot rule out the possibility of the multifocal interictal activity or functional connections between brain areas resulting in the methods to localize at another possible activity region. Indeed, the goodness of dipole fit for Patient 2's MEG data is very low (0.36), which might indicate the presence of other activity outside the resection area. It could also mean that the orientation of the source is exceedingly radial, which makes it hard to detect via MEG but prominent in EEG since the modalities give complementary information about the activity (Dassios et al., 2007; Aydin et al., 2014). This could explain why SHAL1R can detect epilepsy activity in nearby regions of the resection from EEG data. In order to exclude the influence of other brain regions than the cerebral cortex, where the resections are located, on the accuracy of source localization, we also performed source localization in this limited source space without achieving a substantial improvement in accuracy for Patient 2 MEG (Supplementary Materials 1.2).

The reason why we obtain source estimations most often near the boundary of the resection but almost never inside could also be explained by the characteristics of the focal cortical dysplasia (FCDs), the epileptogenic lesions in

these patients. FCD does not have the typical layered cortical structure, therefore potentially leading to a (partially) closed field. FCD might prevent the pyramidal cells from inducing an open electromagnetic field structure whose source can be estimated inside the resection volume (Neugebauer et al., 2022).

As a limitation of this study, one should also note that the localized epileptic source corresponds to an irritative zone, which may not be the epileptogenic zone that guarantees seizure-freeness when removed (Wellmer, 2018). However, the irritative zone could be neighboring the FCD (Neugebauer et al., 2022) and these zones often overlap (Diamond et al., 2023). An epileptogenic zone is a hypothetical concept that cannot be verified because the seizures can come back after years from the surgery (de Tisi et al., 2011; Chen et al., 2016; Jehi et al., 2018). In a lack of better verification measures, we are making an assumption of the epileptic source location based on the resected volume of the brain, relying on the length of the patients' symptom-free period after surgery (Nissen et al., 2016; Hall et al., 2018; Neugebauer et al., 2022). Another limitation is the irritative zone of both patients lay in the cerebral cortex even if mesocortical epilepsy activity is a possibility (Aydin et al., 2014) and an interesting case with its own challenges as the deep sources are usually hard to detect (Krishnaswamy et al., 2017).

However, HAL1R is previously coupled with RAMUS technique to enhance the detectability of deep sources with a promising set of results based on numerical experiments (Lahtinen et al., 2022), and it is shown that sLORETA (as

standardized MNE) can recover even the subcortical originators of somatosensory evoked potentials with equal accuracy as MNE coupled with RAMUS (Rezaei et al., 2021) which lends credence to the possibility that SHALpR could also function in the localization of deep sources. To investigate it slightly further, we conducted a numerical experiment where a focal source is placed on the posterior cingulate cortex (Supplementary Materials 1.1) suggesting that locating deep sources with an error of less than 1 cm is also possible.

Our results support the hypothesis that applying a focal solver yields a greater localization accuracy of focal epilepsy source than a solver providing a sparse and smooth but widespread distribution when the location of the source is estimated by the reconstruction maximum and one originator for the measurement can be assumed reliably. The hypothesis is supported by the volumetrically small resection regions of the patients examined in this study. Moreover, when considering the results of our numerical experiments, standardization seems to be the key to accurate and noise-tolerant estimates in these cases. This finding was anticipated since sLORETA is known to be a reliable method for locating ES. In previously published studies, sLORETA has been found to localize 8 out of 9 epileptogenic zones (Li et al., 2021) and to be equally accurate as connectivity measures to localize an epileptic source based on standard density EEG (Coito et al., 2019), and to provide consistent results in localizing the epileptic generators of four patients suffering from tuberous sclerosis complex (Leal et al., 2008). SHAL1R's obtained localization accuracy of 1 cm together with sparsity can be considered useful in the planning of resection, e.g., to guide non-invasive, invasive epilepsy work-up, retrospective FLAIR-MRI or Zoomed-MRI, iEEG electrode positioning, or skull opening in neurosurgery (Riney et al., 2012; Aydin et al., 2017).

In Neugebauer et al. (2022) the epileptic activity of the same two patients was reconstructed via dipole scans as well as via event-related and averaged beamforming for a range of regularization parameters. Beamforming techniques have been shown to be able to localize the activity with zero localization error within a small interval of regularization values. However, the intervals found were different for Patient 1 than for Patient 2, and neither of the compared techniques had a clear advantage: methods that worked well in the case of Patient 1 produced a poor localization with Patient 2, and some methods worked with EEG but not with MEG data by estimating the ES location to be more than 2.5 cm away from the resection. The localization accuracy of the averaged beamformer was around 10 mm and 5 mm with event-related beamforming via the optimal regularization parameter. The dipole scan was able to localize the epileptic activity with around the same distance to the resection boundary as sLORETA and HAL1R in our study, but it failed with Patient 2 by estimating ES to 3 cm away from the resection volume.

A broader conclusion about the usefulness of the focal standardized solver or standardization in general in localizing focal epilepsy cannot be drawn with this trial data. The sample sizes or difficulty of the patient cases is not enough

to draw conclusions about the superiority between SHAL1R and sLORETA.

This study demonstrated the usefulness of the standardization technique in improving the localization and suppressing the susceptibility to interference caused by measurement noise. The results suggest that the epileptic source can be localized accurately by using a standardized distributed method. In such a case, the accuracy and features of the estimations depend on the used prior model. The original standardized method, sLORETA, is already meritorious, but the case-wise consistency and the resolution of the reconstruction could be improved by using the Laplace prior.

For further investigation, we could apply standardization for an inversion technique with richer structures, e.g., taking the temporal aspect of biopotential signals into account.

6. Conclusions

In this study, we have demonstrated the applicability of the current density standardization on noise robustness and enhancing the epileptic source localization accuracy by coupling it with a hierarchical Bayesian method with conditionally exponential prior. The inverse model allows us to dictate the focality of the solution to match the assumed focality of the true activity. By examining the localization accuracy with two major sparsity inheriting from the degree of the norm in penalty term of the minimization problem, $L1$ and $L2$, we have observed that $L1$ yielding a greater focality matches better with focal epileptic activity obtained from the patients. $L1$ -penalized SHAL1R outperformed compared standardized methods in most of the source localization cases making it a considerable candidate for focal epilepsy localization.

Declaration of competing interest

None of the authors have conflicts of interest to disclose.

Acknowledgement

This study was supported by ERA PerMED project "Personalised diagnosis and treatment for refractory focal paediatric and adult epilepsy (PerEpi)" (AoF number 344712). Joonas Lahtinen's work has been funded by Väisälä Fund. Alexandra Koulouri is supported by the Academy of Finland (project no. 336357, PROFI 6 - TAU Imaging Research Platform). Carsten Wolters was supported by the Bundesministerium für Gesundheit, project ZMI1-2521FSB006, within the ERA PerMed as project ERAPERMED2020-227 PerEpi and by the Deutsche Forschungsgemeinschaft (DFG), project WO1425/10-1. Sampsa Pursiainen is supported by the Academy of Finland Centre of Excellence (CoE) in Inverse Modeling and Imaging 2018–2025 (decision 353089). Wolters and Pursiainen were additionally supported by the DAAD/AoF researcher mobility project (DAAD project 57663920, AoF decision 35497). Funding agencies have no involvement in the collection, analysis, and interpretation of data and in the writing of the manuscript.

Appendix A. SSLOFO Algorithm

Algorithm 1 SSLOFO

Require: source space \mathcal{S} , smoothing range r , space reduction proportion p , noise covariance matrix C .

Use range search to find neighborhood within range r for each source point in \mathcal{S} .

Define the diagonal matrix $P_{ii} = \|L(:, i)\|^{-1}$

$\Phi = \text{Diag}(\mathbf{1})$

$M_\Phi = L^T (LL^T + C)^{-1}$

for $k = 0, \dots, K_{max}$ **do**

$R = M_\Phi L$

$\hat{u} = M_\Phi y$

Compute current power estimation

$J_i = \hat{u}_i^T (R_{II})^{-1} \hat{u}_i$

Use average-based smoothing within range r to obtain smoothed \hat{J}

Set the source space $\mathcal{S} = \{i: \hat{J}_i \geq p \max(\hat{J})\}$

$W = \text{PWDiag}(|\hat{u}|)^{1/2}$

$\Phi = WW^T$

$M_\Phi = \Phi L^T (L\Phi L^T + C)^{-1}$

end for

Appendix B. Derivation of Standardized Hierarchical Adaptive L_p regularization method

The following minimization problem gives sLORETA estimate as the solution for

$$\begin{aligned} \min_{\mathbf{z}} \left\{ \frac{1}{2} (\mathbf{y} - L\mathbf{T}^{-1}\mathbf{z})^T C^{-1} (\mathbf{y} - L\mathbf{T}^{-1}\mathbf{z}) \right\} \\ \text{subject to } \frac{1}{2} \|P^{-1/2} \mathbf{T}^{-1} \mathbf{z}\|^2 \leq t, \end{aligned} \quad (\text{B.1})$$

for every positive t , where T is the inverse of the decomposition of the diagonal or block diagonal resolution matrix, i.e., $T_{II}^2 = R_{II}^{-1}$, due to the symmetry of the matrix T . To standardize the HBM of conditionally exponential prior and a gamma hyperprior (7), substitute $\mathbf{x} = T_{\gamma}^{-1} \mathbf{z}$. Now the posterior maximizing γ constitutes to the minimization problem

$$\begin{aligned} \min_{\gamma} \left\{ \left\| \text{Diag}(\gamma)^{1/p} T_{\gamma}^{-1} \mathbf{z} \right\|_p^p \right\} \\ \text{subject to } \sum_{j=1}^n (\gamma_j \theta - (\kappa + 1/p - 1) \log \gamma_j) \leq t, \end{aligned} \quad (\text{B.2})$$

for all positive t , with the minimizing solution of the form

$$\hat{\gamma}_j = \frac{\kappa + 1/p - 1}{\left\| [T_{\gamma}^{-1}]_{j,I} \mathbf{z}_I \right\|_p^p + \theta} = \frac{\kappa + 1/p - 1}{|x_j|^p + \theta}, \quad (\text{B.3})$$

for every $j = 1, \dots, n$ and I denotes d -tuple of indices corresponding to d -dimensional position in the modelling scheme.

Due to the scaling property of IAS algorithm (Calvetti et al., 2020), the viability of the algorithm is guaranteed.

In the fixed-point iteration, the aim is to find a Gaussian covariance matrix $P^{(k)}$ such that $\|(P^{(k)})^{-1/2} \mathbf{x}\|_2^2 / 2 = \|\text{Diag}(\gamma^{(k)})^{1/p} \mathbf{x}\|_p^p$ for any \mathbf{x} . The Gaussian covariance matrix is an essential part since it is a component of the resolution matrix. This leads to the minimization problem similar to (B.1) with the solution

$$\hat{\mathbf{z}} = T_{\gamma} P^{(k)} L^T (L P^{(k)} L^T + C)^{-1} \mathbf{y} = T_{\gamma} \hat{\mathbf{x}} \quad (\text{B.4})$$

and the power estimation as the following

$$\hat{\mathbf{z}}_I^T \mathbf{z}_I = \hat{\mathbf{x}}_I^T [T_{\gamma}]_{II}^2 \hat{\mathbf{x}}_I = \hat{\mathbf{x}}_I R_{II}^{-1} \hat{\mathbf{x}}_I. \quad (\text{B.5})$$

Appendix C. Algorithm of Standardized Hierarchical Adaptive L_p Regularization (SHALpR)

Here we present the algorithm to calculate the reconstruction via Standardized Hierarchical Adaptive L_p Regularization (SHALpR). Next, we take a look at the mathematical

Algorithm 2 Hierarchical Adaptive Lasso for the standardized algorithm

Require: hyperpriors κ and θ , noise covariance matrix C , prior degree p , $\gamma^{(0)} < \|L^T y\|_{\infty}$, tolerance ϵ_{tol} , primal variable $x^{(0)} = 0$, $u^{old} = x^{(0)}$

for $k = 0, \dots, K_{max}$ **do**

do

▷ Solve the Lasso problem

$$D = \text{diag} \left(\frac{\gamma_i^{(k)}}{\epsilon + |u_i^{old}|^p} \right)$$

$$R = D^{-1} L^T (L D^{-1} L^T + C)^{-1} L$$

▷ Calculate

resolution matrix

$$\hat{u} = D^{-1} L^T (L D^{-1} L^T + C)^{-1} y$$

$$\mathbf{z} = L\hat{u} - y \text{ and } \lambda_i = \gamma_i^{(k)} \text{ for } i = 1, \dots, N$$

$$f(\hat{u}) = \frac{1}{2} \|L\hat{u} - y\|_2^2 + \sum_{i=1}^N \lambda_i |\hat{u}_i|^p \text{ } \triangleright \text{Primal problem,}$$

for $p = 1$ detailed presentation in Appendix C.1

$\tau = \min \left\{ \frac{\lambda_i}{|L^T z|_i} \text{ for } i = 1, \dots, N \right\}$ and $\nu = \tau z$ ▷ Dual feasible

$$g(\nu) = -0.5 \nu^T \nu - \nu^T y$$

▷ Dual problem

$$\eta = f(\hat{u}) - g(\nu)$$

▷ Duality gap

$$u^{old} = \text{Diag}(R)^{-1/2} \hat{u}$$

▷ Update

sLORETA-weighted solution

while $\eta/g(\nu) > \epsilon_{tol}$ ▷ Stop if the duality gap less than threshold

$x^{(k+1)} = \hat{u}$ ▷ Update the solution for the Adaptive Hierarchical Lasso

$$\gamma_i^{(k+1)} = \frac{\kappa + 1}{\theta + |x_i^{(k+1)}|^p}, \text{ for } i = 1, \dots, N$$

end for

motivations behind the presented dual problem-based stopping criterion.

Appendix C.1. Stopping Criterion for Lasso Problem-Duality Gap

In this section, we give a derivation of the dual problem of the lasso problem and its duality gap used in the solution of the ℓ_1 -norm minimization problem (LASSO):

$$\min_{\mathbf{x} \in \mathbb{R}^n} \left\{ \frac{1}{2} \|\mathbf{L}\mathbf{x} - \mathbf{y}\|_2^2 + \sum_{i=1}^n \lambda_i |x_i| \right\}, \quad (\text{C.1})$$

where $L \in \mathbb{R}^{m \times n}$. In particular, for the estimation of a robust overall stopping criterion for the LASSO problem, we can employ the duality gap which is defined as the difference between the values of functional (C.1) with its Lagrange dual function (Boyd and Vandenberghe, 2004). The Lagrange dual function is always concave and yields lower bounds on the optimal value of the problem (C.1) which can be used as a non-heuristic criterion for the termination of an algorithm (Boyd and Vandenberghe, 2004).

We derive a Lagrange dual by introducing a new variable $\mathbf{z} \in \mathbb{R}^m$ and the equality constraint $\mathbf{z} = \mathbf{L}\mathbf{x} - \mathbf{y}$. The functional in (C.1) can be written with the equal expression

$$\min_{(\mathbf{x}, \mathbf{z})} \left\{ \frac{1}{2} \mathbf{z}^T \mathbf{z} + \sum_{i=1}^n \lambda_i |x_i| \right\} \quad \text{subject to } \mathbf{z} = \mathbf{L}\mathbf{x} - \mathbf{y}. \quad (\text{C.2})$$

The Lagrangian of (C.2) is

$$\mathcal{L}(\mathbf{x}, \mathbf{z}, \mathbf{v}) = \frac{1}{2} \mathbf{z}^T \mathbf{z} + \sum_{i=1}^n \lambda_i |x_i| + \mathbf{v}^T (\mathbf{L}\mathbf{x} - \mathbf{y} - \mathbf{z}), \quad (\text{C.3})$$

where $\mathbf{v} \in \mathbb{R}^m$. We estimate the Lagrange dual function $g: \mathbb{R}^m \rightarrow \mathbb{R}$ by minimizing the Lagrangian over (\mathbf{x}, \mathbf{z})

$$\begin{aligned} g(\mathbf{v}) &= \inf_{(\mathbf{x}, \mathbf{z})} \left\{ \frac{1}{2} \mathbf{z}^T \mathbf{z} + \sum_{i=1}^n \lambda_i |x_i| + \mathbf{v}^T (\mathbf{L}\mathbf{x} - \mathbf{y} - \mathbf{z}) \right\} \\ &= \inf_{\mathbf{z}} \left\{ \frac{1}{2} \mathbf{z}^T \mathbf{z} - \mathbf{v}^T \mathbf{z} \right\} + \inf_{\mathbf{x}} \left\{ \sum_{i=1}^n \lambda_i |x_i| + \mathbf{v}^T (\mathbf{L}\mathbf{x}) \right\} - \mathbf{v}^T \mathbf{y}. \end{aligned} \quad (\text{C.4})$$

From the previous equations, we have that

$$\min_{(\mathbf{x}, \mathbf{z}) \in C} \left\{ \frac{1}{2} \mathbf{z}^T \mathbf{z} + \sum_{i=1}^n \lambda_i |x_i| \right\} = \min_{(\mathbf{x}, \mathbf{z}) \in C} \mathcal{L}(\mathbf{x}, \mathbf{z}, \mathbf{v}) \geq g(\mathbf{v}), \quad (\text{C.5})$$

where $C = \{\mathbf{z} \in \mathbb{R}^m, \mathbf{x} \in \mathbb{R}^n | \mathbf{z} = \mathbf{L}\mathbf{x} - \mathbf{y}\}$ is a feasible set. This implies that the dual function (C.4) yields lower bounds for the optimal values of problem (C.2) for feasible points \mathbf{x} and \mathbf{z} . This bound has a practical meaning if we can make sure that the dual problem is $g(\mathbf{v}) > -\infty$ for some \mathbf{v} . An important property of problem $L1$ -norm is that for an arbitrary \mathbf{x} , we can derive an easily computed bound on the sub-optimality of \mathbf{x} , by constructing a dual feasible point \mathbf{v} (Kim et al., 2007).

From equation (C.4) we derive the Lagrange dual of problem (C.1)

$$\begin{aligned} &\text{maximize } g(\mathbf{v}) = -0.5 \mathbf{v}^T \mathbf{v} - \mathbf{v}^T \mathbf{y} \\ &\text{subject to } \lambda_i \geq \left| \left[\mathbf{L}^T \mathbf{v} \right]_i \right| \text{ for } i = 1, \dots, n, \end{aligned} \quad (\text{C.6})$$

and a dual feasible point \mathbf{v} needs to satisfy the constraints of (C.6). Similarly as in (Koh et al., 2007), we construct the dual feasible point

$$\mathbf{v} = \tau \mathbf{z}, \text{ where } \tau = \min \left\{ \frac{\lambda_i}{\left| \left[\mathbf{L}^T \mathbf{z} \right]_i \right|} \text{ for } i = 1, \dots, n \right\} \quad (\text{C.7})$$

and $\mathbf{z} = \mathbf{L}\mathbf{x} - \mathbf{y}$. The non-negative difference between the objective value of problem (C.1) and $g(\mathbf{v})$ is the so-called duality gap, denoted by

$$\eta = \frac{1}{2} \|\mathbf{L}\mathbf{x} - \mathbf{y}\|_2^2 + \sum_{i=1}^n \lambda_i |x_i| - g(\mathbf{v}) \geq 0. \quad (\text{C.8})$$

The algorithm terminates when the fraction of the duality gap η over the value of the dual function $g(\mathbf{v})$ falls below a tolerance ϵ_{tol} (see further notes in (Kim et al., 2007)).

Appendix C.2. Bound for Lasso parameter λ

Proposition 1. If $\lambda > \|\mathbf{L}^T \mathbf{y}\|_\infty$ then the unique minimizer is given by $\mathbf{x} = \mathbf{0}$. If $\lambda < \|\mathbf{L}^T \mathbf{y}\|_\infty$, then each solution is different from zero.

Proof. Convexity and coercivity immediately imply the existence of a minimizer. Let $\lambda > \|\mathbf{L}^T \mathbf{y}\|_\infty$, then

$$\begin{aligned} J(\mathbf{x}) &= \frac{1}{2} \|\mathbf{L}\mathbf{x} - \mathbf{y}\|_2^2 + \lambda \|\mathbf{x}\|_1 \\ &= \frac{1}{2} \|\mathbf{L}\mathbf{x}\|_2^2 + \frac{1}{2} \|\mathbf{y}\|_2^2 + \lambda \|\mathbf{x}\|_1 - \mathbf{x}^T \mathbf{L}^T \mathbf{y} \\ &\geq \frac{1}{2} \|\mathbf{L}\mathbf{x}\|_2^2 + \frac{1}{2} \|\mathbf{y}\|_2^2 + (\lambda - \|\mathbf{L}^T \mathbf{y}\|_\infty) \|\mathbf{x}\|_1 \\ &\geq \frac{1}{2} \|\mathbf{y}\|_2^2 = J(\mathbf{0}), \end{aligned}$$

with inequality only for $\mathbf{x} = \mathbf{0}$. Hence, $\mathbf{x} = \mathbf{0}$ is the unique minimizer. In the case where $\lambda < \|\mathbf{L}^T \mathbf{y}\|_\infty$ we can choose $\mathbf{x} = \epsilon \mathbf{L}^T \mathbf{y}$ with $\epsilon > 0$ sufficiently small to verify that there exists a \mathbf{x} yielding a functional value lower than $\frac{1}{2} \|\mathbf{y}\|_2^2$. \square

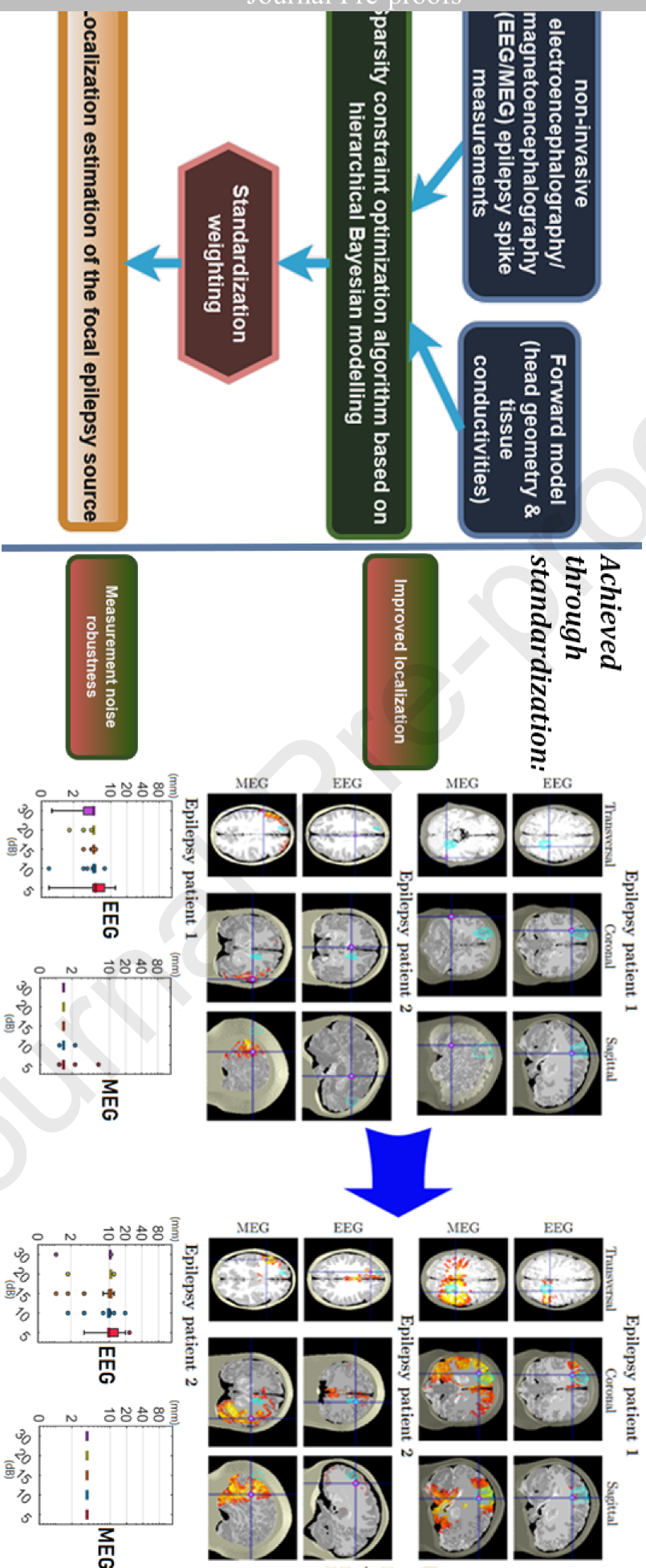
References

- Alarcón, G., Binnie, C.D., García Seoane, J.J., Martín Miguel, M.C., Fernández Torre, J.L., Polkey, C.E., Guy, C.N., 1999. Mechanisms involved in the propagation of interictal epileptiform discharges in partial epilepsy. *Electroencephalogr. clin. neurophysiol.* 50, 259–.
- Attal, Y., Schwartz, D., 2013. Assessment of subcortical source localization using deep brain activity imaging model with minimum norm operators: a meg study. *PLoS one* 8, e59856–e59856.
- Aydin, Ü., Rampp, S., Wollbrink, A., Kugel, H., Cho, J.H., Knösche, T.R., Grova, C., Wellmer, J., Wolters, C.H., 2017. Zoomed MRI guided by combined EEG/MEG source analysis: A multimodal approach for optimizing presurgical epilepsy work-up and its application in a multi-focal epilepsy patient case study. *Brain topogr.* 30, 417–433.
- Aydin, Ü., Vorwerk, J., Küpper, P., Heers, M., Kugel, H., Galka, A., Hamid, L., Wellmer, J., Kellinghaus, C., Rampp, S., Wolters, C.H., 2014. Combining EEG and MEG for the reconstruction of epileptic activity using a calibrated realistic volume conductor model. *PLoS one* 9, e93154–e93154.
- Bast, T., Boppel, T., Rupp, A., Harting, I., Hoechstetter, K., Fauser, S., Schulze-Bonhage, A., Rating, D., Scherg, M., 2006. Noninvasive source localization of interictal EEG spikes: Effects of signal-to-noise ratio and averaging. *J. clin. neurophysiol.* 23, 487–497.

- Bauer, M., Pursiainen, S., Vorwerk, J., Köstler, H., Wolters, C.H., 2015. Comparison study for Whitney (Raviart–Thomas)-type source models in finite-element-method-based EEG forward modeling. *IEEE Trans. Biomed. Eng.* 62, 2648–2656.
- Baumgartner, C., Pataia, E., Lindinger, G., Deecke, L., 2000. Magnetoencephalography in focal epilepsy. *Epilepsia (Copenhagen)* 41, S39–S47.
- Boyd, S., Vandenberghe, L., 2004. Convex Optimization. Cambridge University Press. URL: <http://www.stanford.edu/~boyd/cvxbook/bv-cvxbook.pdf>.
- Brodbeck, V., Spinelli, L., Lascano, A.M., Wissmeier, M., Vargas, M.I., Vulliemoz, S., Pollo, C., Schaller, K., Michel, C.M., Seeck, M., 2011. Electroencephalographic source imaging: a prospective study of 152 operated epileptic patients. *Brain (London, Engl. : 1878)* 134, 2887–2897.
- Cai, C., Chen, J., Findlay, A.M., Mizuiri, D., Sekihara, K., Kirsch, H.E., Nagarajan, S.S., 2021. Clinical validation of the champagne algorithm for epilepsy spike localization. *Front. Hum. Neurosci.* 15, 642819–642819.
- Calvetti, D., Hakula, H., Pursiainen, S., Somersalo, E., 2009. Conditionally Gaussian hypermodels for cerebral source localization. *SIAM J. on Imag. Sci.* 2, 879–909. doi:10.1137/080723995.
- Calvetti, D., Pragliola, M., Somersalo, E., Strang, A., 2020. Sparse reconstructions from few noisy data: analysis of hierarchical bayesian models with generalized gamma hyperpriors. *Inverse probl.* 36, 25010–.
- Calvetti, D., Somersalo, E., Strang, A., 2019. Hierarchical bayesian models and sparsity: ℓ_2 -magic. *Inverse probl.* 35, 35003–.
- Chen, H., Modur, P.N., Barot, N., Van Ness, P.C., Agostini, M.A., Ding, K., Gupta, P., Hays, R., Mickey, B., 2016. Predictors of postoperative seizure recurrence: A longitudinal study of temporal and extratemporal resections. *Epilepsy res. trat.* 2016, 7982494–7.
- Coito, A., Biethahn, S., Tepperberg, J., Carboni, M., Roelcke, U., Seeck, M., Mierlo, P., Gschwind, M., Vulliemoz, S., 2019. Interictal epileptogenic zone localization in patients with focal epilepsy using electric source imaging and directed functional connectivity from low-density EEG. *Epilepsia open* 4, 281–292.
- Conte, F., Legros, B., Van Paesschen, W., Avbersek, A., Muglia, P., Depondt, C., 2018. Long-term seizure outcomes in patients with drug resistant epilepsy. *Seizure* 62, 74–78. URL: <https://www.sciencedirect.com/science/article/pii/S1059131118304990>, doi:https://doi.org/10.1016/j.seizure.2018.09.020.
- Dale, A.M., Liu, A.K., Fischl, B.R., Buckner, R.L., Belliveau, J.W., Lewine, J.D., Halgren, E., 2000. Dynamic statistical parametric mapping: combining fmri and meg for high-resolution imaging of cortical activity. *Neuron (Cambridge, Mass.)* 26, 55–67.
- Dannhauer, M., Lanfer, B., Wolters, C.H., Knösche, T.R., 2011. Modeling of the human skull in EEG source analysis. *Hum. Brain Mapp.* 32, 1383–1399. doi:10.1002/hbm.21114.
- Dassios, G., Fokas, A.S., Hadjiloizi, D., 2007. On the complementarity of electroencephalography and magnetoencephalography. *Inverse probl.* 23, 2541–2549.
- Daubechies, I., DeVore, R., Fornasier, M., Güntürk, C.S., 2010. Iteratively reweighted least squares minimization for sparse recovery. *Commun. on pure applied mathematics* 63, 1–38.
- Diamond, J.M., Withers, C.P., Chapeton, J.I., Rahman, S., Inati, S.K., Zaghloul, K.A., 2023. Interictal discharges in the human brain are travelling waves arising from an epileptogenic source. *Brain* 146, 1903–1915. URL: <https://doi.org/10.1093/brain/awad015>, doi:10.1093/brain/awad015.
- Dümpelmann, M., Ball, T., Schulze-Bonhage, A., 2012. sLORETA allows reliable distributed source reconstruction based on subdural strip and grid recordings. *Hum. Brain Mapp.* 33, 1172–1188.
- Elvetun, O.L., Nielsen, B.F., 2021. A regularization operator for source identification for elliptic pdes. *Inverse probl. imaging (Springfield, Mo.)* 15, 599–.
- Engel, J., 1996. Surgery for seizures. *The New Engl. journal medicine* 334, 647–653.
- Engel Jr, J., Rausch, R., Lieb, J.P., Kuhl, D.E., Crandall, P.H., 1981. Correlation of criteria used for localizing epileptic foci in patients considered for surgical therapy of epilepsy. *Ann. neurol.* 9, 215–224.
- Eom, T.H., Shin, J.H., Kim, Y.H., Chung, S.Y., Lee, I.G., Kim, J.M., 2016. Distributed source localization of interictal spikes in benign childhood epilepsy with centrotemporal spikes: A standardized low-resolution brain electromagnetic tomography (sLORETA) study. *J. clin. neurosci.* 38, 49–54.
- Feng, R., Hu, J., Pan, L., Wu, J., Lang, L., Jiang, S., Gu, X., Guo, J., Zhou, L., 2016. Application of 256-channel dense array electroencephalographic source imaging in presurgical workup of temporal lobe epilepsy. *Clin. neurophysiol.* 127, 108–116.
- Flandin, G., Friston, K.J., 2019. Analysis of family-wise error rates in statistical parametric mapping using random field theory. *Hum. Brain Mapp.* 40, 2052–2054.
- Fuchs, M., Wagner, M., Köhler, T., Wischmann, H.A., 1999. Linear and nonlinear current density reconstructions. *J. clin. neurophysiol.* 16, 267–295.
- Fuchs, M., Wagner, M., Wischmann, H.A., Köhler, T., Theißen, A., Drenckhahn, R., Buchner, H., 1998. Improving source reconstructions by combining bioelectric and biomagnetic data. *Electroencephalogr. clin. neurophysiol.* 107, 93–111.
- Grech, R., Cassar, T., Muscat, J., Camilleri, K.P., Fabri, S.G., Zervakis, M., Xanthopoulos, P., Sakkalis, V., Vanrumste, B., 2008. Review on solving the inverse problem in eeg source analysis. *J. Neuroeng. Rehabil.* 5, 25–25.
- Greenblatt, R., Ossadtchi, A., Pflieger, M., 2005. Local linear estimators for the bioelectromagnetic inverse problem. *IEEE Trans. Signal Process.* 53, 3403–3412.
- de Gooijer-van de Groep, K.L., Leijten, F.S., Ferrier, C.H., Huiskamp, G.J., 2013. Inverse modeling in magnetic source imaging: Comparison of MUSIC, SAM(g2), and sLORETA to interictal intracranial EEG. *Hum. brain mapping* 34, 2032–2044.
- Grova, C., Daunizeau, J., Lina, J.M., Bénar, C., Benali, H., Gotman, J., 2006. Evaluation of eeg localization methods using realistic simulations of interictal spikes. *NeuroImage (Orlando, Fla.)* 29, 734–753.
- Hall, M.B., Nissen, I.A., van Straaten, E.C., Furlong, P.L., Witton, C., Foley, E., Seri, S., Hillebrand, A., 2018. An evaluation of kurtosis beamforming in magnetoencephalography to localize the epileptogenic zone in drug resistant epilepsy patients. *Clin. neurophysiol.* 129, 1221–1229.
- Haufe, S., Nikulin, V.V., Ziehe, A., Müller, K.R., Nolte, G., 2008. Combining sparsity and rotational invariance in eeg/meg source reconstruction. *NeuroImage (Orlando, Fla.)* 42, 726–738.
- Hauk, O., Wakeman, D.G., Henson, R., 2011. Comparison of noise-normalized minimum norm estimates for MEG analysis using multiple resolution metrics. *NeuroImage (Orlando, Fla.)* 54, 1966–1974.
- He, Q., Rezaei, A., Pursiainen, S., 2019. Zeffiro user interface for electromagnetic brain imaging: a gpu accelerated fem tool for forward and inverse computations in matlab. *Neuroinformatics* doi:10.1007/s12021-019-09436-9.
- Hämäläinen, M., Ilmoniemi, R., 1994. Interpreting magnetic fields on the brain: minimum norm estimates. *Med. Biol. Eng. Comput.* 32, 35–42.
- Jehi, L., Yehia, L., Peterson, C., Niazi, F., Busch, R., Prayson, R., Ying, Z., Bingaman, W., Najm, I., Eng, C., 2018. Preliminary report: Late seizure recurrence years after epilepsy surgery may be associated with alterations in brain tissue transcriptome. *Epilepsia open* 3, 299–304.
- Kantorovich, L.V., 1940. On one effective method of solving certain classes of extremal problems. *Akad. Nauk USSR* 28, 212–215.
- Kim, S.J., Koh, K., Lustig, M., Boyd, S., Gorinevsky, D., 2007. An interior-point method for large-scale ℓ_1 -regularized least squares. *IEEE J. Sel. Top. Signal Process.* 1, 606–617. doi:10.1109/JSTSP.2007.910971.
- Kirsch, H., Robinson, S., Mantle, M., Nagarajan, S., 2006. Automated localization of magnetoencephalographic interictal spikes by adaptive spatial filtering. *Clin. neurophysiol.* 117, 2264–2271.
- Knowlton, R.C., Elgavish, R., Howell, J., Blount, J., Burneo, J.G., Faught, E., Kankirawatana, P., Riley, K., Morawetz, R., Worthington, J., Kuzniecky, R.I., 2006. Magnetic source imaging versus intracranial electroencephalogram in epilepsy surgery: A prospective study. *Ann. neurol.* 59, 835–842.
- Knösche, T.R., Haueisen, J., 2022. EEG/MEG Source Reconstruction: Textbook for Electro-And Magnetoencephalography. Springer International Publishing AG, Cham.
- Koh, K., Kim, S.J., Boyd, S., 2007. An Interior-Point Method for Large-Scale L1-Regularized Logistic Regression. *J. Mach. Learn. Research* .
- Krishnaswamy, P., Obregon-Henao, G., Ahveninen, J., Khan, S., Babadi, B., Iglesias, J.E., Hämäläinen, M.S., Purdon, P.L., 2017. Sparsity enables

- estimation of both subcortical and cortical activity from MEG and EEG. *Proc. National Acad. Sci. - PNAS* 114, E10465–E10474.
- Lahtinen, J., Koulouri, A., Rezaei, A., Pursiainen, S., 2022. Conditionally exponential prior in focal near- and far-field EEG source localization via randomized multiresolution scanning (ramus). *J. Math. Imag. Vis.* URL: <https://doi.org/10.1007/s10851-022-01081-3>, doi:10.1007/s10851-022-01081-3.
- Lantz, G., Spinelli, L., Seeck, M., de Peralta Menendez, R.G., Sottas, C.C., Michel, C.M., 2003. Propagation of interictal epileptiform activity can lead to erroneous source localizations: A 128-channel EEG mapping study. *J. clin. neurophysiol.* 20, 311–319.
- Leal, A.J., Dias, A.I., Vieira, J.P., Moreira, A., Távora, L., Calado, E., 2008. Analysis of the dynamics and origin of epileptic activity in patients with tuberous sclerosis evaluated for surgery of epilepsy. *Clin. neurophysiol.* 119, 853–861.
- Li, C., Jacobs, D., Hilton, T., Campo, M.d., Chinvarun, Y., Carlen, P.L., Bardakjian, B.L., 2016. Epileptogenic source imaging using cross-frequency coupled signals from scalp eeg. *IEEE Trans. Biomed. Eng.* 63, 2607–2618.
- Li, R., Plummer, C., Vogrin, S.J., Woods, W.P., Kuhlmann, L., Boston, R., Liley, D.T., Cook, M.J., Grayden, D.B., 2021. Interictal spike localization for epilepsy surgery using magnetoencephalography beamforming. *Clin. neurophysiol.* 132, 928–937.
- Lie, O.V., Papanastassiou, A.M., Cavazos, J.E., Szabó, Á.C., 2015. Influence of intracranial electrode density and spatial configuration on interictal spike localization: A case study. *J. clin. neurophysiol.* 32, e30–e40.
- Lin, F.H., Wald, L.L., Ahlfors, S.P., Hämäläinen, M.S., Kwong, K.K., Belliveau, J.W., 2006. Dynamic magnetic resonance inverse imaging of human brain function. *Magn. resonance medicine* 56, 787–802.
- Liu, H., Schimpf, P., Dong, G., Gao, X., Yang, F., Gao, S., 2005. Standardized shrinking LORETA-FOCUSS (SSLOFO): a new algorithm for spatio-temporal EEG source reconstruction. *IEEE Trans. Biomed. Eng.* 52, 1681–1691.
- Lucka, F., Pursiainen, S., Burger, M., Wolters, C.H., 2012. Hierarchical Bayesian inference for the EEG inverse problem using realistic FE head models: Depth localization and source separation for focal primary currents. *NeuroImage* 61, 1364–1382. doi:10.1016/j.neuroimage.2012.04.017.
- Lüders, H.O., Najm, I., Nair, D., Widdess-Walsh, P., Bingman, W., 2006. The epileptogenic zone: general principles. *Epileptic disorders* 8 Suppl 2, S1–S9.
- Miinalainen, T., Rezaei, A., Us, D., Nüßing, A., Engwer, C., Wolters, C.H., Pursiainen, S., 2019. A realistic, accurate and fast source modeling approach for the EEG forward problem. *NeuroImage* 184, 56–67.
- Mohd Zulkifly, M.F., Lehr, A., van de Velden, D., Khan, A., Focke, N.K., Wolters, C.H., Paulus, W., 2022. Directionality of the injected current targeting the P20/N20 source determines the efficacy of 140 Hz transcranial alternating current stimulation (tACS)-induced aftereffects in the somatosensory cortex. *PLoS one* 17, e0266107–e0266107.
- Mouthaan, B.E., Rados, M., Boon, P., Carrette, E., Diehl, B., Jung, J., Kimiskidis, V., Kobulashvili, T., Kuchukhidze, G., Larsson, P.G., Leitinger, M., Ryylin, P., Rugg-Gunn, F., Seeck, M., Vulliemoz, S., Huiskamp, G., Leijten, F.S., Van Eijnsden, P., Trinka, E., Braun, K.P., 2019. Diagnostic accuracy of interictal source imaging in presurgical epilepsy evaluation: A systematic review from the e-pilepsy consortium. *Clin. neurophysiol.* 130, 845–855.
- Murakami, H., Wang, Z.I., Marashly, A., Krishnan, B., Prayson, R.A., Kakisaka, Y., Mosher, J.C., Bulacio, J., Gonzalez-Martinez, J.A., Bingaman, W.E., Najm, I.M., Burgess, R.C., Alexopoulos, A.V., 2016. Correlating magnetoencephalography to stereo-electroencephalography in patients undergoing epilepsy surgery. *Brain (London, Engl. : 1878)* 139, 2935–2947.
- Mégevand, P., Spinelli, L., Genetti, M., Brodbeck, V., Momjian, S., Schaller, K., Michel, C.M., Vulliemoz, S., Seeck, M., 2014. Electric source imaging of interictal activity accurately localises the seizure onset zone. *J. neurology, neurosurg. psychiatry* 85, 38–43.
- Neugebauer, F., Antonakakis, M., Unnwongse, K., Parpaley, Y., Wellmer, J., Rampp, S., Wolters, C.H., 2022. Validating EEG, MEG and combined MEG and EEG beamforming for an estimation of the epileptogenic zone in focal cortical dysplasia. *Brain sciences* 12, 114–.
- Nissen, I., Stam, C., Citroen, R., Reijneveld, J., Hillebrand, A., 2016. Pre-operative evaluation using magnetoencephalography: Experience in 382 epilepsy patients. *Epilepsy res.* 124, 23–33.
- Oostenveld, R., Fries, P., Maris, E., Schoffelen, J.M., 2011. Fieldtrip: Open source software for advanced analysis of MEG, EEG, and invasive electrophysiological data. *Comput. intelligence neurosci.* 2011, 156869–9.
- Otsubo, H., Chitoku, S., Ochi, A., Jay, V., Rutka, J.T., Smith, M.L., Elliott, I.M., Snead, O.C., 2001. Malignant rolandic-sylvian epilepsy in children: Diagnosis, treatment, and outcomes. *Neurology* 57, 590–596.
- Pascual-Marqui, R.D., 2002. Standardized low-resolution brain electromagnetic tomography (sLORETA): technical details. *Methods find. exp. clin. pharmacol.* 24, 5–12.
- Pascual-Marqui, R.D., 2007. Discrete, 3D distributed, linear imaging methods of electric neuronal activity. part 1: exact, zero error localization. *arXiv.org*.
- Plummer, C., Harvey, A.S., Cook, M., 2008. EEG source localization in focal epilepsy: Where are we now? *Epilepsia (Copenhagen)* 49, 201–218.
- Pursiainen, S., Vorwerk, J., Wolters, C.H., 2016. Electroencephalography (EEG) forward modeling via H(div) finite element sources with focal interpolation. *Phys. Med. Biol.* 61, 8502.
- Rampp, S., Stefan, H., Wu, X., Kaltenhäuser, M., Maess, B., Schmitt, F.C., Wolters, C.H., Hamer, H., Kasper, B.S., Schwab, S., Doerfler, A., Blümcke, I., Rössler, K., Buchfelder, M., 2019. Magnetoencephalography for epileptic focus localization in a series of 1000 cases. *Brain* 142, 3059–3071. URL: <https://doi.org/10.1093/brain/awz231>, doi:10.1093/brain/awz231.
- Rezaei, A., Antonakakis, M., Piastra, M., Wolters, C.H., Pursiainen, S., 2020. Parametrizing the conditionally gaussian prior model for source localization with reference to the p20/n20 component of median nerve sep/sef. *Brain sciences* 10, 934–.
- Rezaei, A., Lahtinen, J., Neugebauer, F., Antonakakis, M., Piastra, M.C., Koulouri, A., Wolters, C.H., Pursiainen, S., 2021. Reconstructing subcortical and cortical somatosensory activity via the ramus inverse source analysis technique using median nerve sep data. *NeuroImage (Orlando, Fla.)* 245, 118726–118726.
- Rice, J.K., Rorden, C., Little, J.S., Parra, L.C., 2013. Subject position affects EEG magnitudes. *NeuroImage (Orlando, Fla.)* 64, 476–484.
- Riney, C.J., Chong, W.K., Clark, C.A., Cross, J.H., 2012. Voxel based morphometry of flair mri in children with intractable focal epilepsy: Implications for surgical intervention. *Eur. J. Radiol.* 81, 1299–1305.
- Rosenow, F., Lüders, H., 2001. Presurgical evaluation of epilepsy. *Brain (London, Engl. : 1878)* 124, 1683–1700.
- Roth, B.J., Balish, M., Gorbach, A., Sato, S., 1993. How well does a three-sphere model predict positions of dipoles in a realistically shaped head? *Electroencephalogr. clin. neurophysiol.* 87, 175–184.
- Rubner, Y., Tomasi, C., Guibas, L., 1998. A metric for distributions with applications to image databases, in: Sixth International Conference on Computer Vision (IEEE Cat. No.98CH36271), IEEE. pp. 59–66.
- Saha, S., Nesterets, Y.I., Tahtali, M., Gureyev, T.E., 2015. Evaluation of spatial resolution and noise sensitivity of sLORETA method for EEG source localization using low-density headsets. *Biomed. phys. & eng. express* 1, 45206–.
- Sakuma, K., Sekihara, K., Hashimoto, I., 1999. Neural source estimation from a time-frequency component of somatic evoked high-frequency magnetic oscillations to posterior tibial nerve stimulation. *Clin. neurophysiol.* 110, 1585–1588.
- Samuelsson, J.G., Peled, N., Mamashli, F., Ahveninen, J., Hämäläinen, M.S., 2021. Spatial fidelity of MEG/EEG source estimates: A general evaluation approach. *NeuroImage (Orlando, Fla.)* 224, 117430–117430.
- Scherg, M., Ille, N., Bornfleth, H., Berg, P., 2002. Advanced tools for digital EEG review:: Virtual source montages, whole-head mapping, correlation, and phase analysis. *J. clin. neurophysiol.* 19, 91–112.
- Schimpf, P.H., Liu, H., 2008. Localizing sources of the p300 using ica, sslofo, and latency mapping. *J. Biomech. Biomed. Biophys. Eng.* 2, 1–11.
- Sekihara, K., Abraham-Fuchs, K., Stefan, H., Hellstrand, E., 1996. Suppression of background brain activity influence in localizing epileptic spike sources from biomagnetic measurements. *Brain topogr.* 8, 323–328.
- Sekihara, K., Nagarajan, S.S., 2008. Adaptive Spatial Filters for Electromagnetic Brain Imaging. Series in Biomedical Engineering. 1st ed. 2008. ed., Springer Berlin Heidelberg, Berlin, Heidelberg.

- Sekihara, K., Sahani, M., Nagarajan, S.S., 2005. Localization bias and spatial resolution of adaptive and non-adaptive spatial filters for MEG source reconstruction. *NeuroImage (Orlando, Fla.)* 25, 1056–1067.
- Shiraishi, H., Stufflebeam, S.M., Knake, S., Ahlfors, S.P., Sudo, A., Asahina, N., Egawa, K., Hatanaka, K., Kohsaka, S., Saitoh, S., Grant, P.E., Dale, A.M., Halgren, E., 2005. Dynamic statistical parametric mapping for analyzing the magnetoencephalographic epileptiform activity in patients with epilepsy. *J. child neurol.* 20, 363–369.
- Siegel, S., Tukey, J.W., 1960. A nonparametric sum of ranks procedure for relative spread in unpaired samples. *J. Am. Stat. Assoc.* 55, 429–445.
- Sohrabpour, A., He, B., 2021. Exploring the extent of source imaging: Recent advances in noninvasive electromagnetic brain imaging. *Cur. opin. biomed. eng.* 18, 100277–.
- Soler, A., Moctezuma, L.A., Giraldo, E., Molinas, M., 2022. Automated methodology for optimal selection of minimum electrode subsets for accurate EEG source estimation based on genetic algorithm optimization. *Sci. rep.* 12, 11221–11221.
- de Tisi, Jane, B., Bell, Gail S, M., Peacock, Janet L, P., McEvoy, Andrew W, F., Harkness, William FJ, F., Sander, Josemir W, P., Duncan, John S, P., 2011. The long-term outcome of adult epilepsy surgery, patterns of seizure remission, and relapse: a cohort study. *The Lancet (British edition)* 378, 1388–1395.
- Unnwongse, K., Rampp, S., Wehner, T., Kowoll, A., Parpaley, Y., von Lehe, M., Lanfer, B., Rusiniak, M., Wolters, C., Wellmer, J., 2023. Validating EEG source imaging using intracranial electrical stimulation. *Brain commun.* 5, fcad023–fcad023.
- Vanrumste, B., Van Hoey, G., Van de Walle, R., D’Havé, M.R., Lemahieu, I.A., Boon, P.A., 2002. Comparison of performance of spherical and realistic head models in dipole localization from noisy EEG. *Med. eng. & phys.* 24, 403–418.
- Vaserstein, L.N., 1969. Markov processes over denumerable products of spaces, describing large systems of automata. *Probl. Inform. Transm.* 5, 47–52.
- Vatta, F., Meneghini, F., Esposito, F., Mininel, S., Di Salle, F., 2010. Realistic and spherical head modeling for EEG forward problem solution: A comparative cortex-based analysis. *Comput. Intell. Neurosci.* 2010, 972060–11.
- van de Velden, D., Heide, E.C., Bouter, C., Bucerius, J., Riedel, C.H., Focke, N.K., 2023. Effects of inverse methods and spike phases on interictal high-density EEG source reconstruction. *Clin. neurophysiol.* 156, 4–13.
- Vorwerk, J., Aydin, Ü., Wolters, C.H., Butson, C.R., 2019. Influence of head tissue conductivity uncertainties on EEG dipole reconstruction. *Front. Neurosci.* 13. URL: <https://www.frontiersin.org/articles/10.3389/fnins.2019.00531>, doi:10.3389/fnins.2019.00531.
- Wagner, M., Fuchs, M., Kastner, J., 2004. Evaluation of slorta in the presence of noise and multiple sources. *Brain topogr.* 16, 277–280.
- Wellmer, J., 2018. Lesion focused radiofrequency thermocoagulation of bottom-of-sulcus focal cortical dysplasia type IIb: Conceptual considerations with regard to the epileptogenic zone. *Epilepsy res.* 142, 143–148.
- Wellmer, J., Parpaley, Y., Rampp, S., Popkirov, S., Kugel, H., Aydin, Ü., Wolters, C.H., von Lehe, M., Voges, J., 2016. Lesion guided stereotactic radiofrequency thermocoagulation for palliative, in selected cases curative epilepsy surgery. *Epilepsy res.* 121, 39–46.
- Wipf, D., Nagarajan, S., 2009. A unified bayesian framework for MEG/EEG source imaging. *NeuroImage (Orlando, Fla.)* 44, 947–966.
- Zijlmans, M., Zweiphenning, W., van Klink, N., 2019. Changing concepts in presurgical assessment for epilepsy surgery. *Nat. rev. Neurol.* 15, 594–606.



AUTHOR CONCURRENCE FORM CLINICAL NEUROPHYSIOLOGY

Official Organ of the International Federation of Clinical Neurophysiology (IFCN)
<http://www.journals.elsevier.com/clinical-neurophysiology>

Prof. Ulf Ziemann
Editor-in-Chief

Instructions:

1. Each submission to Clinical Neurophysiology needs a filled out Author Concurrence Form. Please fill in the Title of the manuscript below.
2. Collect signatures from all authors.
- 3a. Scan the form and submit it together with the paper. The submission item is Author Agreement.
- 3b. If this is not an option, please fax the form to the Editorial Office: +31-20-485-3881.

Title of the Manuscript: Reconstructing focal epileptic source using hierarchical Bayesian methods with standardization: localization and noise robustness of hierarchical adaptive L_p regression

A signature below certifies compliance with the following statements.

Copyright Transfer: In consideration of the acceptance of the above manuscript for publication, the copyright is transferred to IFCN and administered by Elsevier. All proprietary rights other than copyright (such as patent rights) are reserved to the author(s), as well as the right to use original figures and tables in future works, provided full credit is given to the original publication. If the manuscript is work prepared by employee(s) of the United Kingdom or the United States government as part of their official duties, copyright cannot be fully transferred to the IFCN, and authors must check the appropriate box below.

- This manuscript was written in the course of employment by the United Kingdom and it is subject to Crown copyright.
- This manuscript was written in the course of employment by the United States Government and it is not subject to copyright in the United States.

Authorship Responsibility:

The submission is a truthful, original work without fabrication, fraud or plagiarism, and contains no libellous or unlawful statements.

It has not been published previously except in abstract form.

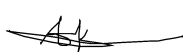
The manuscript is not under consideration for publication, nor will it be submitted for publication, elsewhere until a final decision has been made by this journal.


The undersigned certify that each author has participated sufficiently in the work to take responsibility for its truthfulness and validity, has read the complete manuscript, and concurs with its content.

Conflict of interest disclosure:

All funding sources supporting this work are acknowledged. The authors will disclose to the editor any pertinent financial interests associated with the manufacture of any drug or product described in this manuscript.

ALL AUTHORS MUST SIGN

Author <u>Joonas Lahtinen</u>	Date <u>07.08.2023 09:22:46 (UTC +0300)</u>
Author <u></u>	Date <u>04.08.2023 17:43:21 (UTC +0300)</u>
Author <u>Alexandra Koulouri</u>	Date _____

Author	Stefan Rampp	Stefan Rampp	Date	07.08.2023 14:11:39 (UTC +0300)
Author	Jörg Wellmer	Jörg Wellmer	Date	06.08.2023 17:41:52 (UTC +0300)
Author	Carsten Wolters	Carsten Wolters	Date	07.08.2023 13:21:49 (UTC +0300)
Author		Sampsa Pursiainen	Date	04.08.2023 15:53:01 (UTC +0300)

Journal Pre-proofs